Lehrstuhl E15
Physik-Department

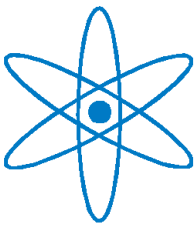

Calibration and Efficiency Determination of the Borexino Muon Veto Based on the First Realtime Measurements of ^{7}Be Solar Neutrinos

Diplomarbeit

Timo Lewke

5. Dezember 2007

Technische Universität München

To my parents
and my brother

Abstract

In this thesis the field of view is focused on the inner and outer muon veto of the solar neutrino experiment Borexino. Work for calibration and maintenance of the Outer Detector as well as efficiency determination of muon identification was performed.
In the first chapter a short introduction to the Standard Solar Model is given. Next, neutrino physics in the Standard Model and beyond, concerning neutrino mass, mixing and scattering, is introduced.
The second chapter describes the setup of the Borexino experiment and reports first results after a exposure of 47.4 days. A ^7Be neutrino rate of $47 \pm 7(stat.) \pm 12(syst.) \frac{counts}{100t \cdot day}$ could be reported.
Chapter three describes the installation of a pulser system for the Outer Detector electronics and its implementation to the data evaluation software Echidna, in order to distinguish between damaged channels and dead PMTs.
In chapter four, an introduction to a new implemented part, treating the Outer Detector electronics, of the simulation software bx_elec is given. Using the simulated data it will be possible to verify the measured and reconstructed data.
The fifth chapter handles different possibilities to treat the Inner Detector as a muon veto. Therefore different possible cuts are introduced and their efficiencies are presented.
Chapter six is dedicated to the efficiency of the inner and outer muon veto. First the different cuts described in the previous chapter are combined, and an efficiency of the inner muon veto is determined. Then, the efficiency of the Outer Detector, used as a muon veto, is determined befor the efficiency of the combined, inner and outer muon veto is calculated.
The last chapter summarizes the results of the previous and gives an outlook for further work that can or has to be done in order to further improve Borexino.

Contents

1 Introduction

The Sun is the most prominent object in our sky. Great efforts have been made to get a better understanding of it. Different models were invented to predict the behaviour of its interior. The one, considered as the most probable is the so called Standard Solar Model (SSM).

1.1 The Standard Solar Model

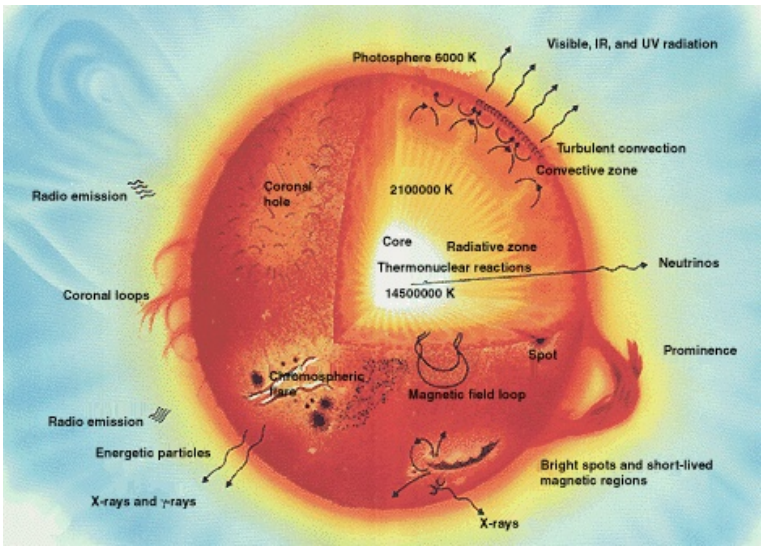

Figure 1.1: Cross section of the Sun showing some processes of the SSM [NASA].

In the Sun the fusion reactions take place in the core. These reactions (Figure 1.2) provide the Sun with energy and prevent it from gravitational collapse. Because of opacity of the Sun matter, photons that are generated in the core need several thousend years to get to the surface in order to escape. Only neutrinos released in fusion reactions are able to escape immediately and therefore can supply information about the ongoing situation of the Sun right now. Hence they are very interesting for astrophysics.
One of the most important aspects of the SSM is to describe this energy production. There are different nuclear fusion reactions powering the Sun (Figure 1.2).
The fundamental one has two different starting points. The first one is the direct *pp*-fusion of two protons, the second one is the so called *pep*-reaction, where two protons fuse with an electron. The *pp*-chain has a higher percentage in the enrgy production than the *pep*-chain. The further process can be devided into four different channels, whereas the last, the $ppIV$-chain, sometimes is called *hep*-chain. The different rates to the contribution are

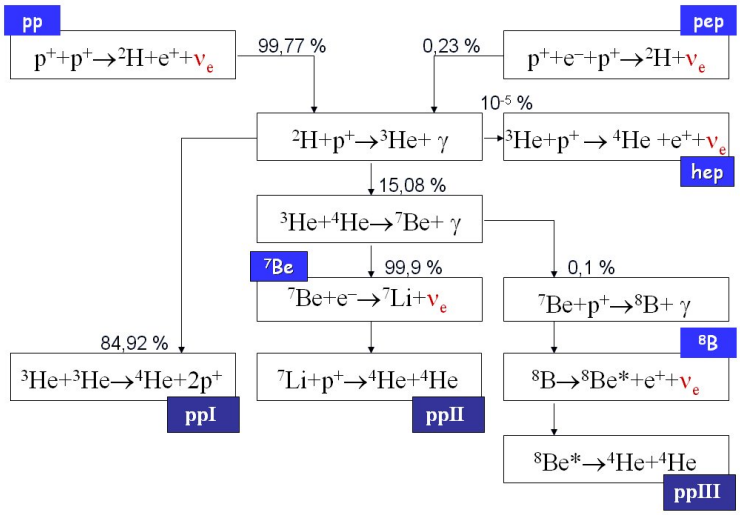

Figure 1.2: The different pp- and the pep-chain-reactions of the SSM.

given in Figure 1.2. For the three dominant *pp*-chains, the total nuclear fusion reaction is equal:

$$p + p + p + p \longrightarrow {}^4He + 2e^+ + 2\nu_e \tag{1.1}$$

The total energy release of each chain summarizes to $Q = 26.73MeV$, but the generated neutrinos have different energy. For every branch the first neutrino generated is a ν_e^{pp}-neutrino. The further process depends on the following reactions:

- *pp*I: another neutrino from *pp*: ν_e^{pp} with a maximum energy of $0.42MeV$
- *ppII*: a neutrino from electron capture: $\nu_e^{^7Be}$ with a maximum energy of $0.86MeV$
- *ppIII*: a neutrino from β^+-decay: $\nu_e^{^8B}$ with a maximum energy of $15MeV$

The remaining energy for the solar heat production depends on the respective fusion reaction.

In addition there is another process contributing to the fusion reactions in the Sun. The *CNO*-cycle, also known as the Bethe-Weizsäcker-cycle (see Figure 1.3).

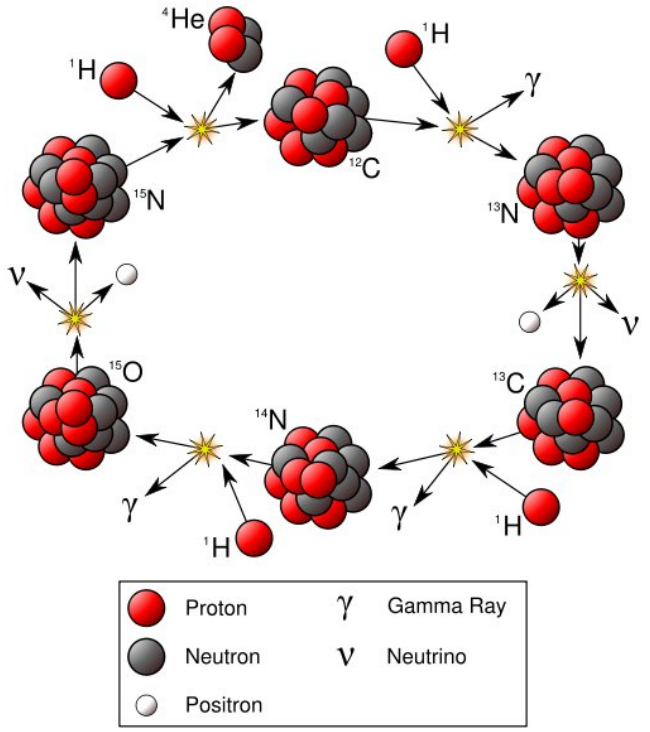

Figure 1.3: The CNO-I-cycle of the SSM [WikNe].

The name derives from the elements taking part in this reaction: Carbon, Nitrogen and Oxygen.
The overall equation that describes the CNO-I-cycle is equal to the pp one, with an additional ^{12}C atom:

$$^{12}C + 4p \longrightarrow {}^{12}C + {}^{4}He + 2e^{+} + 2\nu_e \tag{1.2}$$

This reaction is inhibited by high Coulomb barriers. Hence, a very high temperature is needed to start this cycle. That's why it is suppressed in small stars like the Sun. Only approximately 1.7% of the ^4He is produced via the CNO-I-cycle in the Sun. Theoretically there would be another three CNO-cycles, but they are suppressed strongly and therefore only take place in heavy stars.

The part of energy, E_ν, the neutrinos carry away is just small, it averages at about 2% of Q. The produced energy that powers the electromagnetic luminosity of Sun is $Q^* = Q - E_\nu \approx 0.98 \cdot Q$. The measured luminosity of the Sun is $L = 3.84 \cdot 10^{33} \frac{erg}{s}$. With the Energy Q^* and the distance of Sun and Earth $d = 149.6 \cdot 10^6 km$, the total solar neutrino flux Φ_ν on Earth can be calculated as

$$\Phi_\nu \approx \frac{2}{4\pi d^2} \cdot \frac{L}{Q^*} = 6.6 \cdot 10^{10} \frac{1}{cm^2 s} \tag{1.3}$$

The fluxes and energies for the single solar neutrino emissions are listed in Table 1.1. The spectrum of the neutrino flux is shown in Figure 1.4.

Neutrino Branch	Φ_ν $[\frac{1}{cm^2 s}]$	E_ν $[MeV]$	$E_{\nu,max}$ $[MeV]$
pp	$(5.95 \pm 0.06) \cdot 10^{10}$	0.2668	0.423
^7Be	$(4.77 \pm 0.48) \cdot 10^9$	0.863	0.863
^7Be	$(4.77 \pm 0.48) \cdot 10^9$	0.386	0.386
^8B	$(5.05^{+1.01}_{-0.81}) \cdot 10^6$	6.735± 0.036	≈ 15
pep	$(1.40 \pm 0.02) \cdot 10^8$	1.445	1.445
hep	$9.3 \cdot 10^3$	9.628	18.778
^{13}N	$(5.48^{+1.15}_{-0.93}) \cdot 10^8$	0.7063	1.1982± 0.0003
^{15}O	$(4.80^{+1.20}_{-0.91}) \cdot 10^8$	0.9964	1.7317± 0.0005
^{17}F	$(5.63 \pm 1.41) \cdot 10^6$	0.9977	1.7364± 0.0003

Table 1.1: Energy and flux of the different neutrinos [Lud05]. The two values for the ^7Be-Neutrino derive from the ground state and the $487keV$ excited state of ^7Li.

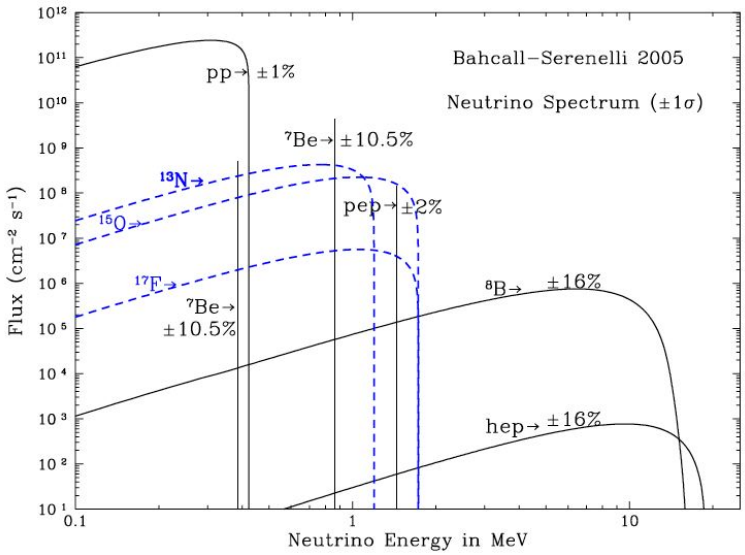

Figure 1.4: Calculated neutrino flux of the SSM taken from [BahWP]. The black spectrum is generated by the *pp*-reaction, the dashed blue one by the CNO-cycle.

As it can be seen, the neutrinos flux plays an important role in the SSM and therefore solar neutrino experiments are important. Therefore a short glance should be spent on their physics and their general behaviour.

1.2 Neutrinos in the Standard Model and Beyond

In the Standard Modell (SM) of particle physics neutrinos are arranged in 3 generations, like e^-, μ and τ. They can interact via the weak interaction, using the neutral (NC) or charged (CC) current. The currents are described by the exchange bosons, $W^\pm$ for CC and Z^0 for NC. The weak interaction has an underlying SU(2) symmetry. Because of neutrinos

being left-handed particles, they form a doublet with the left-handed part of their associated leptons:

$$\Psi_L = \begin{pmatrix} e_L \\ \nu_L \end{pmatrix}, \Psi_R = e_R \tag{1.4}$$

1.2.1 Neutrino Mass

Left- and right-handed fields can be described as the Weyl spinors of the Dirac field:

$$\Psi_{\substack{L \\ R}} = \frac{1 \mp \gamma_5}{2}\Psi \tag{1.5}$$

Hence a mass term in the Lagrangian for neutrinos can be imposed:

$$-\mathcal{L}_\nu = m(\overline{\Psi_R}\Psi_L + \overline{\Psi_L}\Psi_R) \tag{1.6}$$

Because in the SM Ψ_R does not exist for neutrinos, they have consequently no mass in this description. There are diffrent models to introduce mass terms [FukYa]:

- There is the possibility of the excistence of a right handed component of the neutrino ν_R. The created Lagrangian

  $$-\mathcal{L}_{\nu_D} = m(\overline{\Psi_R}\Psi_L + h.c.) \tag{1.7}$$

  leads to so called "Dirac mass" term m.

- In case of the Majorana theory, the neutrino is assumed as its own antiparticle. Therefor the charge-conjugated field $\Psi^c = C\gamma^0\Psi$ is introduced. A Lagrangian

  $$-\mathcal{L}_{\nu_M} = M(\overline{\Psi_L^c}\Psi_L + h.c.). \tag{1.8}$$

  where M is the "Majorana mass" of a neutrino that can be introduced.

Both approaches go beyond the SM. There is no ν_R or $\overline{\nu_L}$ present in the SM. Just as well as the lepton conversation is violated for the case of a Majorana mass.
A third method to introduce masses for neutrinos is the so called "seesaw mechanism".

- It combines both, the Dirac and Majorana theory and leads to a mass Lagrangian

  $$-\mathcal{L} = m\overline{\nu_R}\nu_L + \frac{M}{2}\overline{\nu_R^c}\nu_R + h.c. \tag{1.9}$$

  The mass matrix U

  $$U = \begin{pmatrix} 0 & m \\ m & M \end{pmatrix} \tag{1.10}$$

  can be diagonalised, what procures mixing between left and right handed neutrinos and gives the effective mass Lagrangian:

  $$-\mathcal{L}_{eff} = \frac{m^2}{2M}\overline{\nu_L^c}\nu_L \tag{1.11}$$

  In this way a very small left-handed neutrino mass m_ν can be established:

  $$m_\nu \approx \frac{m^2}{M} \tag{1.12}$$

Experiments
A good way for directly measuring the neutrino mass is to observe the kinematics of a β-decay. The energy spectrum of the emitted $e^{\pm}$ can be described using the Kurie-Description as a function of energy [Povh]

$$K(E_e) = \sqrt{\frac{\frac{dN(E_e)}{dE_e}}{F(Z', E_e)E_e\sqrt{E_e^2 - m_e^2c^4}}}, \tag{1.13}$$

where $F(Z^{'}, E_e)$ is the Fermi-Funktion, E_e, m_e are energy and mass of the electron and $Z^{'}$ is the rest of the atomic number. For $m_\nu = 0$, $K(E_e)$ is simplified to

$$K(E_e) \propto \sqrt{(E_0 - E_e)\sqrt{(E_0 - E_e)^2 - m_\nu^2c^4}}. \tag{1.14}$$

For $m_\nu \neq 0$ there is a deviation at the β-endpoint at high energies (see Figure 1.5). The

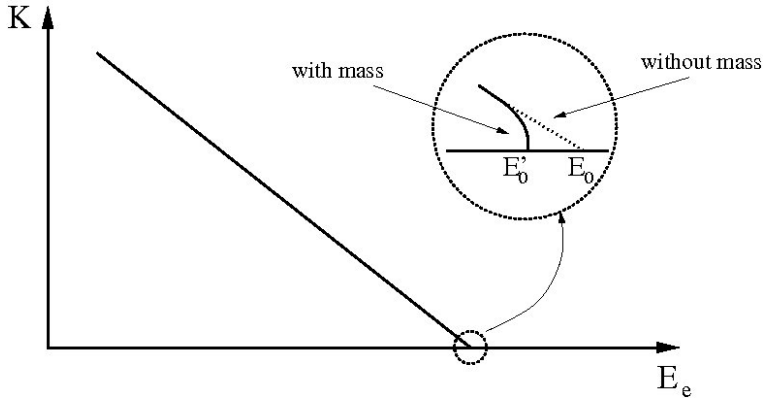

Figure 1.5: Kurie-Description ploted as a function of energy for the two cases of no neutrino masses and neutrino masses. The deviation in the endpoint corresponds to m_ν.

difference in the endpoint accords the neutrino mass:

$$E_0^{'} = E_0 - m_\nu c^2 \tag{1.15}$$

E_0 can be found by the interpolation of the straight line cutting the abscissa. $E_0^{'}$ is gained from experiments, e.g. from KATRIN [KatLi],[KatHp]. Today the best upper boundary for neutrino masses was determined by the Mainz Neutrino Mass Experiment as $m_{\nu_e} \leq 2.2eV$ [KatLi].
Other experiments use neutrino less double beta decay to measure the mass limits, e.g. CUORE/CUORICINO [Cuore].

1.2.2 Neutrino Mixing

Vacuum Oscillations
Assuming neutrino masses m, flavour oscillations in vacuum have to be regarded. The weak interaction eigenstates ν_α, $\alpha = e, \mu, \tau$, are mixtures of the mass eigenstates ν_i, $i = 1, 2, 3$.

Equivalent to the hadronic CKM matrix, a transformation matrix can be introduced, that describes the portions of the 3 mass eigenstates in the 3 flavour states [FukYa]:

$$|\nu^{\alpha}\rangle_t = \sum_i U_{\alpha i} e^{-iE_i t} |\nu'^{i}\rangle \tag{1.16}$$

With E_i as energy of an eigenstate and $U_{\alpha i}$ as transformation matrix. Regarding the transition to another eigenstate ν_β the amplitude

$$\langle\nu^{\beta}|\nu^{\alpha}\rangle_t = \sum U_{\alpha i}(U^{\dagger})_{i\beta} e^{-iE_i t} \tag{1.17}$$

can be used with equation (1.16) to calculate the mixing between the two eigenstates:

$$|\nu^{\alpha}\rangle_t \approx e^{-ipt}\{e^{-i\frac{m^{\dagger}m}{2E}t}\}_{\alpha\beta}|\nu^{\beta}\rangle. \tag{1.18}$$

This is the propability to observe a neutrino of flavour α after a time t. In the simplified case of two-flavour oscillations, the transformation matrix can be written as

$$U = \delta_\alpha U' \delta_\beta = \begin{pmatrix} e^{i\alpha} & \\ & e^{-i\alpha} \end{pmatrix} \begin{pmatrix} \cos\theta & \sin\theta \\ -\sin\theta & \cos\theta \end{pmatrix} \begin{pmatrix} e^{i\beta} & \\ & e^{-i\beta} \end{pmatrix}, \tag{1.19}$$

with θ as the mixing angle of two eigenstates. The two phases $\delta_{\alpha,\beta}$ can be combined with the neutrino wave functions, so that the remaining transformation matrix is U'. The transition probability after traveling a distance L then becomes

$$P_{\nu_e \to \nu_\mu}(L) = \sin^2(2\theta) \cdot \sin^2\left(\frac{\Delta m^2}{4E_\nu} L\right). \tag{1.20}$$

Δm^2 is the squared mass difference of the different neutrinos observed. Regarding now all three neutrino flavours, the mixing can be described by equation (1.21).

$$\begin{pmatrix} \nu_e \\ \nu_\mu \\ \nu_\tau \end{pmatrix} = \begin{pmatrix} 1 & 0 & 0 \\ 0 & c_{23} & s_{23} \\ 0 & -s_{23} & c_{23} \end{pmatrix} \begin{pmatrix} c_{13} & 0 s_{13} e^{i\delta} & \\ 0 & 1 & 0 \\ -s_{13}e^{i\delta} & 0 & c_{13} \end{pmatrix} \begin{pmatrix} c_{12} & s_{12} & 0 \\ -s_{12} & c_{12} & 0 \\ 0 & 0 & 1 \end{pmatrix} \begin{pmatrix} \nu_1 \\ \nu_2 \\ \nu_3 \end{pmatrix}, \tag{1.21}$$

where $s_{ij} = \sin\theta_{ij}$, $c_{ij} = \cos\theta_{ij}$. The introduced phase δ accounts for possible CP-violations.

Matter Oscillations

In matter, electron neutrinos can interact via the neutral or the charged current with e^- (Figure 1.6). On the other hand, muon or tau neutrinos can only interact via the neutral current. This difference in the cross-section leads to a maximal conversion of ν_e to $\nu_{\mu,\tau}$ at a critical mass density. This effect first was pointed out by Mikheyev and Smirnov and is named MSW (Mikheyev-Smirnov-Wolfenstein) mechanism. It is believed to be the most attractive solution of the "solar neutrino problem". The effective Hamiltonian is [FukYa]

$$H_{eff} = \frac{G_F}{\sqrt{2}} \overline{\nu_e} \gamma_\mu (1-\gamma_5) \nu_e \overline{e} \gamma_\mu (1-\gamma_5) e. \tag{1.22}$$

An additional electron neutrino mass term

$$\sqrt{2} G_F n_e \tag{1.23}$$

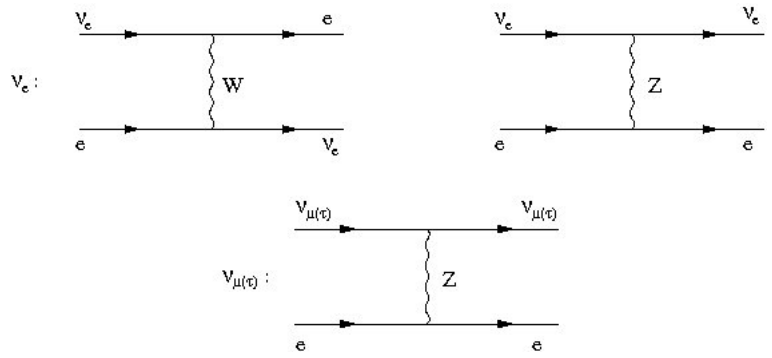

Figure 1.6: Coherent electron-neutrino scattering in matter: Neutral and charged current interactions are possible for ν_e, but only neutral current for $\nu_{\mu,\tau}$. This leads to the introduction of an effective mass term for ν_e.

is added to equation (1.16). n_e is the electron number density in matter and G_F the Fermi coupling constant. The time dependent neutrino wave function is given by the Schrödinger equation:

$$i\frac{d}{dt}\begin{pmatrix}\nu_e\\ \nu_\mu\end{pmatrix} = \begin{pmatrix}-\frac{\Delta m^2}{4E}\cos 2\theta + \sqrt{2}G_F n_e & \frac{\Delta m^2}{4E}\sin 2\theta\\ \frac{\Delta m^2}{4E}\sin 2\theta & \frac{\Delta m^2}{4E}\cos 2\theta\end{pmatrix}\begin{pmatrix}\nu_e\\ \nu_\mu\end{pmatrix} \tag{1.24}$$

The Hamiltonian can be diagonalised

$$\begin{pmatrix}\nu_e\\ \nu_\mu\end{pmatrix} = U\begin{pmatrix}\tilde{\nu_1}\\ \tilde{\nu_2}\end{pmatrix} = \begin{pmatrix}\cos\tilde{\theta} & \sin\tilde{\theta}\\ -\sin\tilde{\theta} & \cos\tilde{\theta}\end{pmatrix}\begin{pmatrix}\tilde{\nu}_1\\ \tilde{\nu}_2\end{pmatrix} \tag{1.25}$$

where $\tilde{\theta}$, the effective mixing angle in matter, is given by

$$\cos 2\tilde{\theta} = \frac{\frac{-A}{\Delta m^2} + \cos 2\theta}{\sqrt{(\frac{A}{\Delta m^2} - \cos 2\theta)^2 + \sin^2 2\theta}} \tag{1.26}$$

The effective mass eigenvalues are then

$$\tilde{m}^2_{\frac{1}{2}} = \frac{A}{2} \mp \frac{1}{2}\sqrt{(A - \Delta m^2\cos 2\theta)^2 + (\Delta m^2)^2\sin^2 2\theta}. \tag{1.27}$$

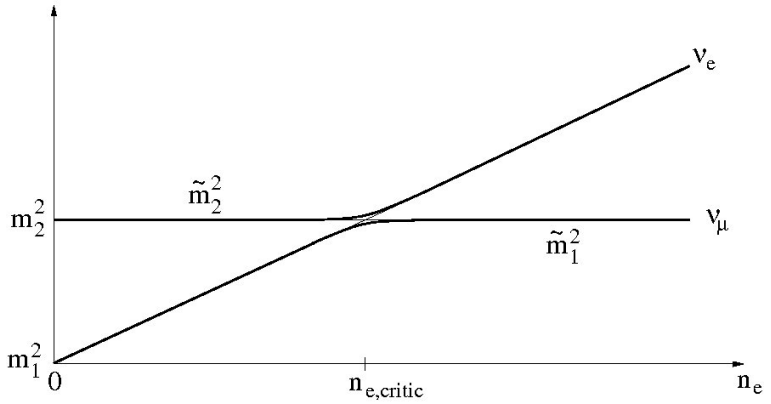

Figure 1.7: Level crossing of the squared neutrino masses in medium (equation (1.27)).

When $\tilde{\theta}$ is maximal, this leads to level crossing (resonance) at $\frac{A}{\Delta m^2} = \cos 2\theta$ (Figure 1.7):

$$n_e = n_{e,critic} = \frac{\Delta m^2 \cos 2\theta}{2\sqrt{2} G_F E}. \tag{1.28}$$

As in the sun adiabatic conversion occurs, a ν_e, that is produced in the region $n_e > n_{e,critic}$ and propagates into the region $n_e < n_{e,critic}$, fully converts into a ν_μ.

Experiments
Experimental evidence for these oscillations have been found in various experiments. For example, MINOS [Minos] measures the neutrino flux. It examines a ν_μ-beam generated at the Fermilab. Two seperate but similar build detectors are used to search for the ν_μ disappearance. One is near the Fermilab and measures the total neutrino flux emitted. The other one is placed $725km$ away. Here also the neutrino flux is measured. The difference in the flux gives a hint to ν_μ disappearance and therefore to neutrino oscillations. The obtained results coincide with the calculated ones, using oscillations. At the far detector 215 events are measured compared to an expectation of 336 [Min06].
As another example, reactor antineutrino oscillations have been observed by KamLand (see Section 1.3) [Kam02]. The setup used for this experiment is similar to the one used by MINOS. Two seperate detectors are used to measure the $\bar{\nu_e}$ disappearance. Also solar neutrino experiments like Kamiokande, SuperKamiokande, SNO, etc. are measuring neutrino disappearance. For example, regarding $\overline{\nu}_e$-flux from the sun, disappearance measurements were performed by KamLAND [Kam03],[Kam04]. These experiments will be described later in detail. Results, achieved by SNO and SuperKamiokande, for the mixing angle θ and the squared neutrino mass differences Δm^2 are presented in Table 1.2.

θ_{12}	θ_{23}	${\Delta m_{12}}^2$	${\Delta m_{23}}^2$
$(32.5^{+1.6}_{-1.7})^\circ$	45°	$(7.1^{+1.0}_{-0.3} \cdot 10^{-5}) eV^2$	$2 \cdot 10^{-3} eV^2$

Table 1.2: Mixing angles and squared neutrino masses by SNO and SuperKamiokande.

1.2.3 ν-Electron Scattering

The elastic scattering of neutrinos on electrons

$$\nu_x + e^- \longrightarrow \nu_x + e^-, \tag{1.29}$$

is an important detection reaction for todays neutrino experiments, with $x = e, \mu, \tau$. All flavours interact via the neutral current. It is crucial to remember that electron neutrinos have an additional interaction possibility [Povh], due to the charged current (Figure 1.6). This leads to a difference in the cross section. Using [FukYa], the differential cross section for all neutrino flavours can be written as

$$\frac{d\sigma}{dT_e'} = \frac{2G_F m_e}{\pi}\left[c_L^2 + c_R^2\left(\frac{E_\nu'}{E_\nu}\right)^2 - c_L c_R \frac{m_e(E_\nu - E_\nu')}{E_\nu^2}\right]. \tag{1.30}$$

With $T_e' = E_\nu - E_\nu'$ as recoil energy of the electron and m_e as its mass. The energy of the neutrino before and after the reaction is given by E_ν, E_ν'. Again G_F is the Fermi coupling constant. The differences, because of different weak interactions, are implemented in the parameters c_L, c_R (see Table 1.3). The total cross section can be calculated:

$$\sigma = \frac{2G_F m_e E_\nu}{\pi}\left[c_L^2 + \frac{1}{3}c_R^2 - \frac{1}{2}c_L c_R \frac{m_e}{E_\nu}\right]. \tag{1.31}$$

The values of the total cross section are summed in Table 1.3. As can be seen, the cross section for electron neutrino scattering is indeed much larger than for muon or tau neutrinos, due to the extra interaction possibility via charged current.

	c_L	c_R	$\sigma\ [10^{-43}\frac{cm^2 E_\nu}{10MeV}]$
$\nu_e e^- \to \nu_e e^-$	$\frac{1}{2} + \sin^2\theta_w$	$\sin^2\theta_w$	0.952
$\nu_{\mu,\tau} e^- \to \nu_{\mu,\tau} e^-$	$-\frac{1}{2} + \sin^2\theta_w$	$\sin^2\theta_w$	0.155
$\overline{\nu}_e e^- \to \overline{\nu_e} e^-$	$\sin^2\theta_w$	$\frac{1}{2} + \sin^2\theta_w$	0.399
$\overline{\nu}_{\mu,\tau} e^- \to \overline{\nu_{\mu,\tau}} e^-$	$\sin^2\theta_w$	$-\frac{1}{2} + \sin^2\theta_w$	0.134

Table 1.3: Coefficients appearing in neutrino-lepton scattering and cross section [FukYa].

1.3 Solar Neutrino Detectors

A short overview of the different techniques for the detection of solar neutrinos is given and corresponding experiments are presented. In Chapter 2, the Borexino detector will be described in detail.
There are three major kinds of detection systems.

- The first is the radiochemical detection of neutrinos. A reaction of the type

$$\nu_e + {}^A_Z Y \longrightarrow {}^A_{Z+1} Y' + e^- \tag{1.32}$$

allows for the detection process. The necessary energy for the capture is accountable for the energy threshold of the detector. Therefore special materials, allowing a very low threshold, have to be used. The reaction product has to be filtered out of the educts once a week and the amount is counted. So the daughter nucleus must have a reasonable lifetime (of about a month), to accumulate. Real time measurement is not possible, only time- and energy-integrated measurement can be performed.

- On the other hand, there are water Čerenkov detectors. Particles, travelling faster than light in the detector, emitt Čerenkov light, whose propagation is similar to the mach cone. A special angle, the Čerenkov-angle, is defined. The produced light rings can be used for a track resolution. Real time measurement is possible, detecting the light with a light sensitive sensor system. The threshold of these kind of detectors is set to $5MeV$ because of their relatively bad light yield. Hence they are limited to ^8B neutrino observation.

- Liquid scintillator detectors. Organic molecules are excited and emitt in the UV-light spectrum. For solar neutrinos, the reaction (1.29) is the most important process. An additional use of wave length shifter can increas the result by preventing self-absorption. The isotropic emission of light allows for the use of detectors that are sensitive to that special spectrum of light. Therefore a very good light yield (up to 50 times better than the Čerenkov detectors) can be achieved. Also a good energy resolution is possible. The threshold, compared to the other detector systems, is very low. Sometimes it is limited by the electronic system that is used or by rdioactive purity. It is important to have low radioactive contamination. The spallation products could influence the measurement. A direct track resolution is not possible.

Radiochemical Detectors
The first solar neutrino detector, was the Homestake Chlorine experiment [Hom98]. In 1970 it was placed in the Homestake Gold Mine, at Lead, South Dakota. The shielding was $1.478km$ of rock ($\approx 4200m.w.e$). The single horizontal steel tank had a diameter of $6.1m$ and a length of $14.6m$. It contained $615t$ of C_2Cl_4. Data taking was performed up to 1996. The detection reaction was

$$\nu_e + {}^{37}Cl \longrightarrow {}^{37}Ar + e^- \tag{1.33}$$

with a threshold of $814keV$. So the experiment was able to detect ^7Be, ^8B and CNO neutrinos. The expected rate was

$$R_{expected} = 7.7^{+1.2}_{-1.0} SNU. \tag{1.34}$$

$SNU = 10^{-36} \frac{events}{second \times target\ nucleus}$ is the Solar Neutrino Unit. The measured event rate [Hom98] was only

$$R_{measured} = (2.56 \pm 0.16[stat.] \pm 0.16[syst.])SNU. \tag{1.35}$$

The differences between theory and experiment gave birth to the Solar Neutrino Problem (SNP), that now is solved by the experimental evidence for neutrino oscillations.

Other projects like SAGE and GALLEX used Gallium instead of Chlorine

$$\nu_e + {}^{71}Ga \longrightarrow {}^{71}Ge + e^-. \tag{1.36}$$

They achieved a better threshold of $233keV$ and thus were sensitive to not yet measured pp-neutrinos. GALLEX [Gal98] target consisted of $30t$ of gallium in a $101t$ solution of $GaCl_3$ acidified in HCl. It was placed in the Gran Sasso National Laboratory (Italy). It measured the integral neutrino flux from 5/1991 to 1/1997. In 5 years of data taking (65 solar runs) an event rate of

$$R_{measured} = (76 \pm 8)SNU \tag{1.37}$$

was measured compared to the prediction of the SSM

$$R_{expected} = 131^{+12}_{-10}SNU. \tag{1.38}$$

Also here the SNP occured.

In 1997 and 1998 GALLEX was transformed into GNO. The intention was to reduce systematic uncertainties and to do a long term measurement. Especially the *pp*-flux of a full solar cycle was of great interest. Because of security problems in the underground laboratory, the project had to be stoped in April 2003. The final results [GNO05] give a rate of

$$R_{measured} = 62.9^{+6.0}_{-5.9}SNU. \tag{1.39}$$

Regarding all data taken, as well by GALLEX as by GNO, the event rate observed is

$$R_{measured} = (69.3 \pm 5.5)SNU. \tag{1.40}$$

Another project using gallium is the SAGE experiment [Sag02]. It is placed at the Baksan Neutrino Observatory in the northern Caucasus mountains of Russia. The target is formed by $50t$ of liquid metallic gallium. Data acquisition started in 1990 and after 12 years of measurement a rate of

$$R_{measured} = 70.8^{+5.3}_{-5.2}[stat.]^{+3.7}_{-3.2}[syst.]SNU \tag{1.41}$$

was published. It is in good agreement with the results from GALLEX+GNO (1.40). Combining the data from SAGE and other solar neutrino projects, the *pp*-neutrino flux that reaches the Earth can be estimated [Sag02] to

$$\Phi_{\nu,Earth} = (4.6 \pm 1.1) \cdot 10^{10} \frac{1}{cm^2 s} \tag{1.42}$$

Taking neutrino oscillations into account, the total emitted *pp*-flux from the Sun is

$$\Phi_{\nu,Sun} = (7.7 \pm 1.8) \cdot 10^{10} \frac{1}{cm^2 s}. \tag{1.43}$$

It is in good agreement with the prediction of the SSM (Table 1.1).

Čerenkov Light and Liquid Scintillator Detectors

The second detector for solar neutrinos was also the first water Čerenkov Detector: KamiokaNDE

[Kam96]. It was placed in the Kamioka mine $200km$ west of Tokio. Using the detection of Čerenkov light emitted by the recoil electrons, it was the first experiment doing neutrino real time measurement. Originally constructed as a nucleon decay experiment it used a cylindrical tank ($15.6m$ diameter and $16m$ height) filled with $3000t$ of pure water as neutrino target. The light was detected by 948 photomuliplier tubes (PMT's) looking at the inner $2140t$ of water. This inner part (inner detector) was seperrated from the outer region (outer detector) by black sheets. The energy threshold was $7.5MeV$ and so ^8B-neutrinos could be observed. For data evaluation, the fiducial volume was set to the innermost $680t$. The runtime of 2079 days (from 1987-1995) covers almost a total solar cycle of eleven years. The flux measured

$$\Phi_{\nu,measured} = (2.80 \pm 0.19[stat.] \pm 0.33[syst.]) \cdot 10^6 \frac{1}{cm^2 s} \tag{1.44}$$

accords to 49%-64% of the theoretical flux (Tabel 1.1). The background could be suppressed, because neutrino events pointed away from the sun. Being able to do the first neutrino track reconstructions, neutrinos could be separated from statistical spread background.

Super-Kamiokande [SuKa2] is the advancement of KamiokaNDE. It consists of a steel tank, $39m$ diameter and $42m$ tall, and has a water capacity of $50000t$. It is divided by a stainless steal framework spaced $2 - 2.5m$ inside the tank walls. A part of the inner detector ($32000t$) is formed by the fiducial volume of $22.5kt$. It is looked at by 11146 PMTs. The outer detector is used as active shielding against external radioactivity from surrounding rock and air. This area of the detector is observed by 1885 outward pointing PMTs. The threshold is $5MeV$. Therefore only ^8B-neutrinos can be detected, like in KamioKANDE. During a data taking of 1496 days the flux for ^8B-neutrinos is

$$\Phi_{\nu,measured} = (2.35 \pm 0.02[stat.] \pm 0.08[sys.]) \cdot 10^6 \frac{1}{cm^2 s}. \tag{1.45}$$

It is in good agreement with the KamiokaNDE results (eq. (1.44)).

SNO [SNO99] was designed as a heavy water detector. It consists of a transparent acrylic sphere with a diameter of $12m$ and has an overburden of $6000m.w.e$. It is fixed by 10 rope loops and contains $1000t$ of heavy water. It is surrounded by a stainless steel strut carrying 9438 inward facing PMT's. The cavity, $22m$ in diameter and $34m$ in height, containing the detector, is filled with purified light water that shields external radioactivity. It also stabilises the whole structure. SNO is the only detector being able to measure the fluxes of all three neutrino flavours via the three possible reactions

$$\nu_x + e^- \longrightarrow \nu_x + e^- \tag{1.46}$$

$$\nu_e + d \longrightarrow e^- + p + p \tag{1.47}$$

$$\nu_x + d \longrightarrow \nu_x + n + p \tag{1.48}$$

The cross section of the neutral current reaction (1.48) is independent of the neutrino flavour and has a threshold of $2.2MeV$. Equation (1.47) measures only the electron neutrinos. Hence SNO is able to measure the total solar neutrino flux as well as the electron neutrino flux. For the ^8B neutrinos the following fluxes are reported [SNO06]:

$$\Phi_{\nu_e} = 1.76^{+0.05}_{-0.05}[stat.]^{+0.09}_{-0.09}[syst.] \cdot 10^6 \frac{1}{cm^2 s} \tag{1.49}$$

$$\Phi_{\nu_\mu+\nu_\tau} = 3.41^{+0.45}_{-0.45}[stat.]^{+0.48}_{-0.45}[syst.] \cdot 10^6 \frac{1}{cm^2 s} \tag{1.50}$$

The results for the ^8B fluxes measured by the three different reactions (1.46), (1.47), (1.48) are also shown in Figure 1.8. The measured data is compared to the predictions of the

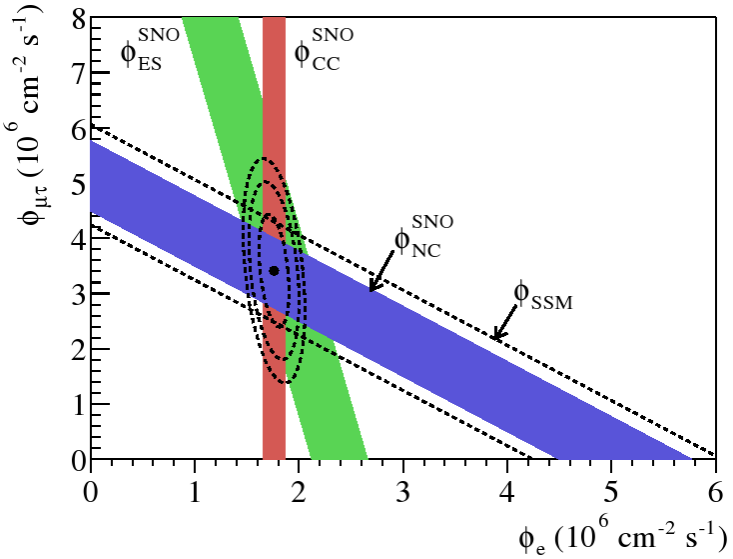

Figure 1.8: Results of SNO [SNO06]. The ^8B fluxes $\Phi_{\nu_\mu+\nu_\tau}$ versus Φ_{ν_e}. Fluxes of the different interactions (1.46), (1.47) and (1.48) are indicated by the filled bands ($\pm 1\sigma$). The prediction of the SSM is shown in dashed lines. Strong evidence for a non-zero flux $\Phi_{\nu_\mu+\nu_\tau}$.

SSM.The result is a strong evidence for a non-zero flux $\Phi_{\nu_\mu+\nu_\tau}$. The sum of both fluxes is in good agreement with the predicted one by the SSM (Table 1.1). A day-night asymmetry in the ν_e flux of $A_e = (7.0 \pm 4.9[stat.]^{+1.3}_{-1.2})\%$ was reported, assuming the total flux as constant. This asymmetry derives from the variation of the measured flux detected at day or night. The MSW effect must be used for neutrinos travelling through the Earth at night, so they have a different flux as by day.

The KamLAND detector was build in the former site of KamiokaNDE. Its design is similar to the Borexino detector. An inner detector filled with $1000t$ of liquid organic scintillator (20% Pseudocumene, 80% Dodecane and $1.5\frac{g}{l}$ PPO) is looked at by 1879 PMTs. An outer detector, used as active muon veto and as background shielding against the external

radioactivity, contains 225 PMTs. The diameter of the outer steel sphere is $18m$. It was originally designed as a reactor neutrino experiment. In order to lower the threshold and to be able to detect the ^7Be-neutrino flux from the Sun, purification was started in spring 2007 [Kam07]. But as reported at TAUP in 2007, the procedure was stoped due to occuring convection problems of the cleaned and uncleaned scintillater.

At the end of this chapter the results of the different experiments are shown in Figure 1.9. The measurement is compared to the associated theoretical prediction by the SSM. One of the important facts is that the total flux measured in SNO agrees with the predicted one, taking also the errors into concern. The other measuered results are smaller than the theoretical predictions due to neutrino oscillations.

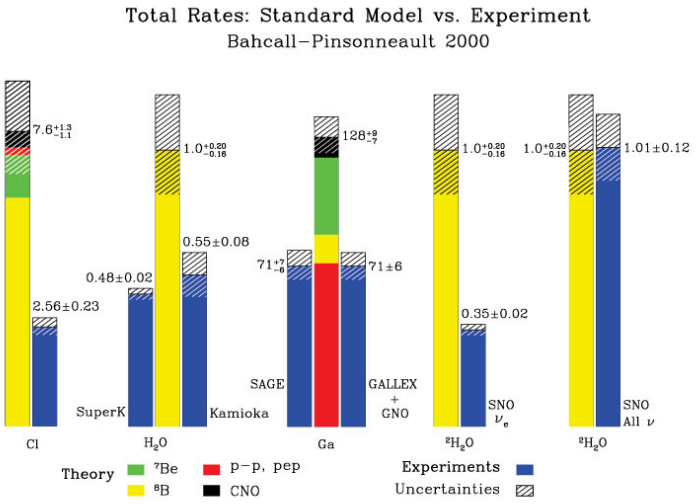

Figure 1.9: Results and predictions of the different solar neutrino experiments [BahWP]. Only the total flux measured by SNO has to be equal with the predicted one.

2 Borexino

All previously mentioned detectors weren't able to perform a real-time measurement of low energetic solar neutrinos like ^7Be, *pep*, CNO or even *pp*-neutrinos. A new detector was planned in the early 90's to do so, Borexino [Bor02][DDa06][BorWP][Tau07][NNN07]. It is a liquid organic scintillator detector sited in the Gran Sasso National Laboratory (LNGS). It has an overburden of approximately 3500 m.w.e. shielding the detector from cosmic rays. Assembly was finished in 2004. End of 2006, the filling of the detector with the liquid scintillator and water started and was accomplished in May 2007. During that process, control runs had been performed to monitor the level of radioactive imparities in the liquid. Data acquisition, then with the fully serviceable detector started on 15.05.2007. Because of the achieved high radioactive purity and the low trigger threshold of approximately $200keV$, Borexino is the first real time experiment that measured the ^7Be neutrino flux (see Section 2.2). However a detailed description of the Borexino design should be given first.

2.1 The Detector

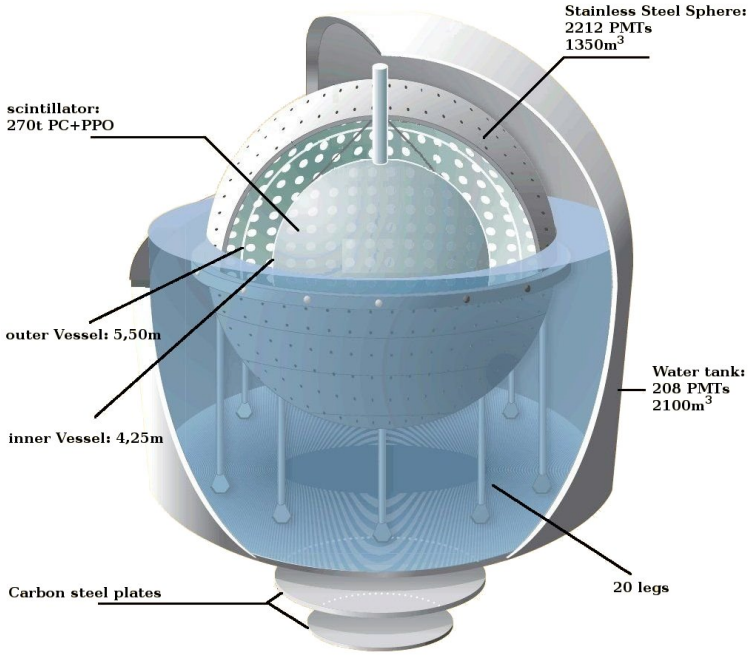

Figure 2.1: Borexino detector [Tau07]. The liquid scintillator in the Inner Vessel of $4.25m$ radius is shielded by several layers of buffer liquid and water.

As can be seen in Figure 2.1, Borexino comprises of several interleaved spheres. The outermost is the watertank that is called Outer Detector (OD). It contains a stainless steel sphere (SSS), that forms the Inner Detector (ID). Later consists of two nylon vessels, Outer Vessel (OV) and Inner Vessel (IV). At the bottom of the detector carbon steel plates are positioned to give a better shielding from the floor. The function of the individual parts is described in the following.

Inner Vessel
The Inner Vessel contains the target volume of the detector. It is composed of transparent

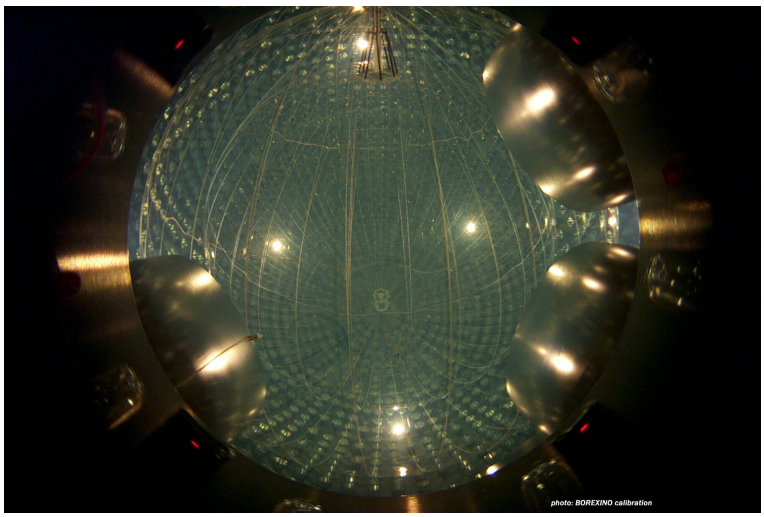

Figure 2.2: View inside the stainless steel sphere: The two nylon vessels filled with buffer liquid and scintillator [BorWP].

nylon that was purified and handled most carefully in order to keep the radioactivity inside the heart of the detector as low as possible. Its diameter is $8.5m$ and its thickness $125\mu m$. It must be absolutely impermeable, because it separates the scintillator from the buffer liquid. The vessel itself is fixed by several strings. Filling and emptying is possible due to steinless steel tubes entering at top and bottom.

Liquid Scintillator
It is filled in the IV. The mixture is composed of pseudocumene (PC 1,2,4-trimethylbenzene, $C_6H_3(CH_3)_3$) and PPO (2,5-diphenyloxazole $C_{15}H_{11}NO$). PC serves as the solvent and represents the target mass for neutrino interactions. Its molekules emit in the UV range. The wave length shifter (fluor) PPO ia added at a concentration of $c = 1.5\frac{g}{l}$ in order to shift the scintillation light to the visible spectrum, where it can leave the liquid scintillator and be detected by the PMTs. In total there is an amount of $270t$ of liquid inside the IV. For data analysis a fiducial volume, consisting of the innermost $100t$ is introduced. The remaining $170t$ serve for self-shielding of the scintillator against external gammas and radioactivity of the Inner Vessel.

Outer Vessel

It has a diameter of approximately $11m$ and the same thickness as the IV. It is fixed at the top and the bottom to the SSS. The intention of this sphere is to prevent radon to enter into the innermost of the detector. Like the Inner Vessel it has to fulfill high requirements regarding radioactive purity.

Buffer Liquid
The buffer liquid is contained outside the IV up to the SSS and acts as shielding device. It also encloses the OV. It has nearly the same density as the scintillator. Otherwise the IV couldn't be kept in place, or would loose its spherical structure. Concidering all that, it was decided to use pure PC with an addition of dimethylphatalate (DMP, $c = 5\frac{g}{l}$). DMP is a quencher that suppresses the scintillation of the PC. In total $1040t$ of buffer liquid are needed.

Stainless Steel Sphere
Everything described so far is placed and mounted inside the SSS. It has a diameter of $13.7m$, a thickness of approximately $10mm$ and is supported by 20 steel legs. The most important role for the sphere is the accommodation of the PMTs for the ID. In total there are 2212 PMTs fixed in the sphere. 1838 of them have a light-concentrator, reflective aluminium cones enlarging the active detection area. In combination with the 374 PMTs without cones the configuration can be used for the identification of muon events (see Section 5.1). Optical fibres are mounted to each PMT which can be used for calibration. A laser signal can be sent to all the PMTs simultaneously via these fibres, providing a single reference signal.

Outer Detector
It is formed by a steel dome. The base has a diameter of $18m$ and the highest point is $17m$ above ground. It is filled with $2400t$ of ultra pure water. For the detection of muons 208 PMTs are mounted inside the OD. Most of them are mounted on the upper half of the SSS pointing outward towards the ceiling and the sides. The remaining are mounted to the floor and the lower inner walls of the OD pointing upwards and inwards. The inner walls of the dome and the outer parts of the SSS are covered with white Tyvek sheets. They will enhance reflectivity ans therefore increase the muon detection possibility. The calibration system for the Outer Detector PMTs is different from the one used in the Inner Detector. Each PMT has its own LED. Via optical fibers the signal can be sent to the individual PMTs.

Organ Pipes
The tubes are mounted to the top of the dome. Through these tubes all the wiring is fed to the inner parts of the detector. The use of these cable ducts assures the nearly absolute darkness inside the detector. It is important to have no light in the detector, because each event just consists of a couple of hundred photons. If light could enter the detector from the outside, it would be totally blind.

2.2 First Results

After two month of data taking (47.4 days of exposure) with the fully equipped detector, the first measurement results of ^7Be neutrinos could be announced [Bor07]. The obtained

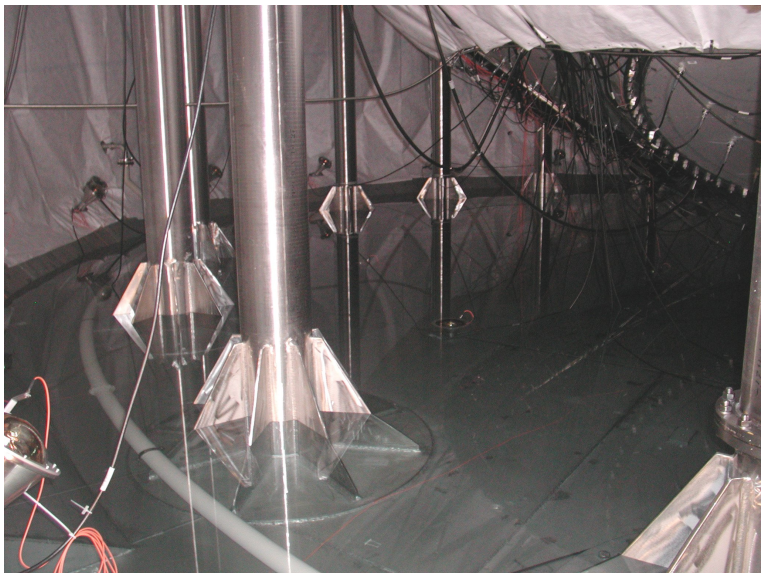

Figure 2.3: Picture showing the outer detector: The inner walls of the dome and the outer side of the Stainless Steel Sphere. It also shows the up and inward pointing PMTs and some of the legs carrying the SSS. The picture was taken during filling process [BorWP].

Figure 2.4: Picture showing the back side of Borexino: The steel dome with some of the organ pipes [BorWP].

raw spectrum, without any cuts performed yet, can be seen in Figure 2.5. The effective light-yield was measured using the data of a spectral fit to the ^{14}C background, which dominates the count rate below $160keV$. The fit yields 500 photoelectrons/MeV. Several cuts are performed to get a clear neutrino signal (Figure 2.6). First all muon events are sub-

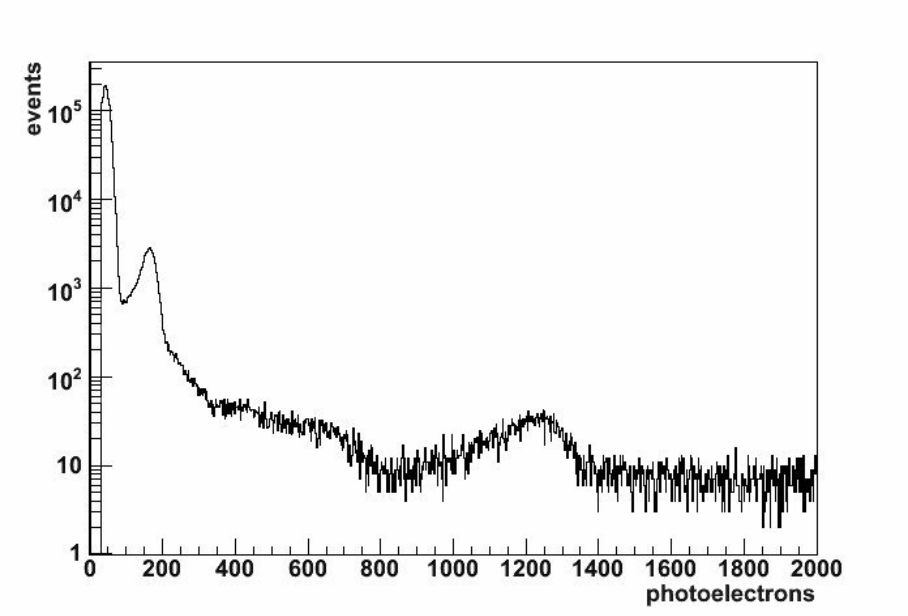

Figure 2.5: Spectrum of the measured events after 2 month of data taking. No cuts were performed at that time [NNN07].

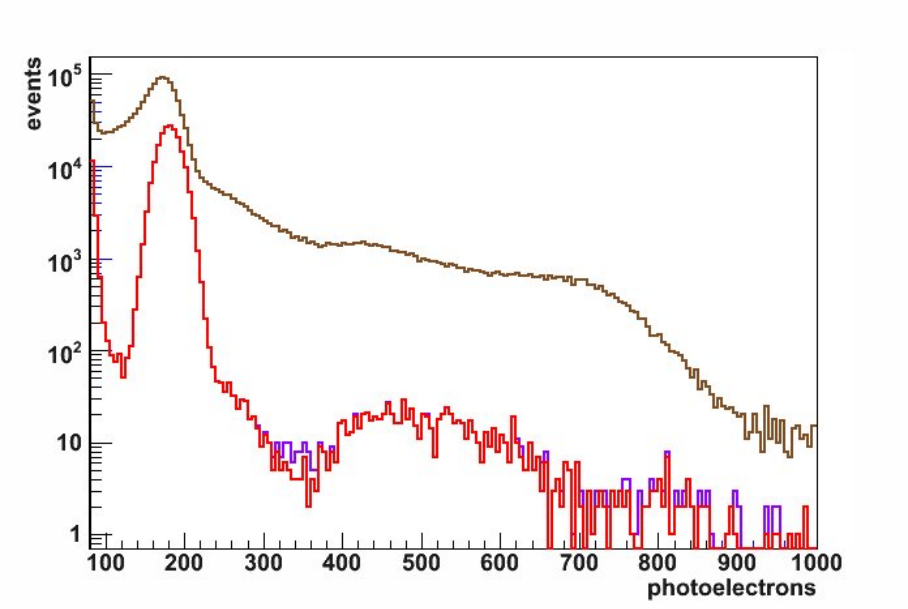

Figure 2.6: The brown line gives the spectrum after a performed muon cut. The purple curve is the result of the restriction to the fiducial volume. The red line shows the spectrum without Rn daughters [NNN07].

stracted, what results in the brown spectrum. After that a fiducial volume cut is performed (purple curve), just regarding the innermost $100t$ of scintillator. This reduces the external

γ background. At last, the Rn daughters occurring before the ^{214}Bi-^{214}Po coincidences are removed (red spectrum in Figure 2.6). The ^{7}Be shoulder is now distinguishable at 330 photoelectrons. Below, the α-peak of ^{210}Po dominates the spectrum. It can be statistically substracted via α/β discrimination. The final result of all performed cuts and a spectral fit for ^{7}Be neutrinos can be seen in Figure 2.7. Here, also fits for the relic background ($^{210}Bi + CNO$, ^{85}Kr, ^{210}Po) are displayed. The energy range is limited to the region of interest, from $260keV$ up to $800keV$.

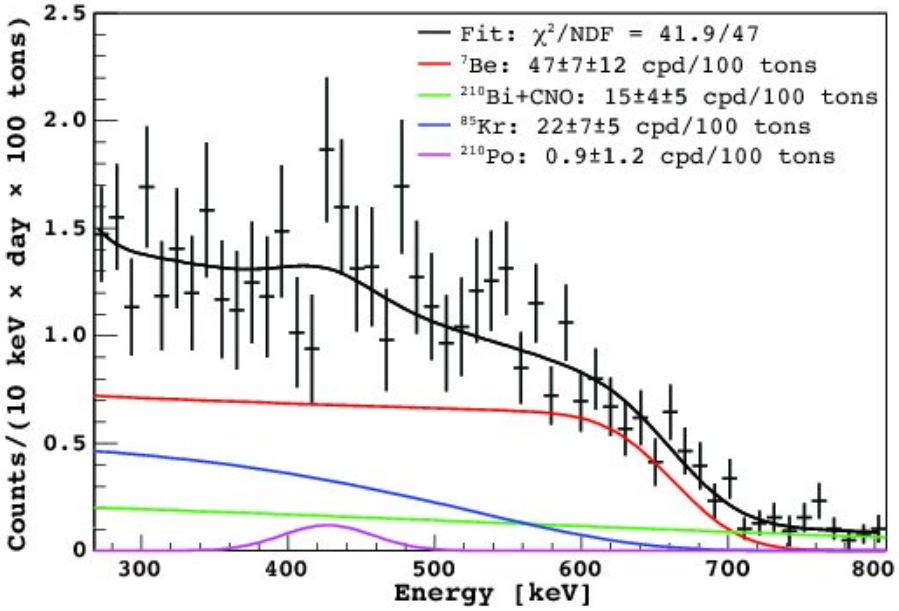

Figure 2.7: Measured spectrum and fits after all cuts have been performed [NNN07].

This is the first real-time measurement of the ^{7}Be solar neutrino spectrum. The best fit to the data is a rate of

$$47 \pm 7(stat.) \pm 12(syst.) \frac{counts}{100t \cdot day} \tag{2.1}$$

The statistical error derives from the short exposure time. It will get better doing more measurements. The systematic uncertainties come from the fiducial volume, varying because of differences in temperature. The results are in good agreement with the expected ones for Borexino of

$$49 \pm 4 \frac{counts}{100t \cdot day}, \tag{2.2}$$

taking the SSM into account. The expected rate without neutrino oscillations would arise to

$$75 \pm 4 \frac{counts}{100t \cdot day}. \tag{2.3}$$

The results of Borexino affirm the assumptions of the SSM and therefore also of the LMA-MSW effect.

3 Pulser System for the Outer Detector

Each PMT in the Outer Detector is coupled to a chain of electronic modules providing it with high voltage and reading out its signals. The pulser system for the OD has been built to be able to distinguish between working and damaged, so to speak dead, channels of the data acquisition (DAQ) system. There was no possibility to check if either the PMT or the electronics was dead, as in both cases there will be no output signals of the specific channel. The new installed pulser system now injects a reference signal into the electronics in order to check if the DAQ chain itself is working. For a better understanding a short overview of the OD electronics is given. After that the pulser system will be described.

3.1 General Overview of the OD Electronics

In Figure 3.1 a shematic overview of the outer detector electronics is shown. In this section a small introduction to the electronics and its function is given.

1. **Patch-Panel**: Here the coaxial cables arriving from the PMTs are mounted. They all have the same length, so each signal has the same run time for each PMT. The signal arriving is forwarded to the HVD (see 2.) by junction cables (SHV). The length of each SHV is $2m$.

2. **HVD**: These are the high voltage decouplers that seperate the AC signal of the PMTs from the HV powering them. Each board contains 24 channels. Every HVD is powered by the **HV Mainframe**, located at the bottom of the rack. The signal of the PMTs arrives at the backside of the HVD. The pulser system is implemented to each boards output on the front side. The outgoing signal then is sent to the QTC-boards.

3. **QTC-boards**: It is the abbreviation for the charge-to-time-converter-boards. These front-end boards are powered by the VME-crate they are mounted in. They process the PMT signal by converting the analog signal to a logic pulse with a length proportional to the collected charge. There are three different outputs, connected to the scalers, the MTB-board and the TDC-boards. The QTC-boards form the most important part for the electronics simulation discussed in Chapter 4.

4. **Scalers**: They are shown in yellow in Figure 3.1 and are placed at the bottom of the left side rack. The output signal is used to give a realtime view of the the PMT rates. They can be accessed via a web interface, to check if everything is working correctly. The scalers don't interact with the data evaluation.

5. **MTB**: The muon trigger board. Its responsiblity is to decide if is a signal above threshold corresponds to a muon. In this case, it issues a trigger signal to the main DAQ and the whole detector is read out.

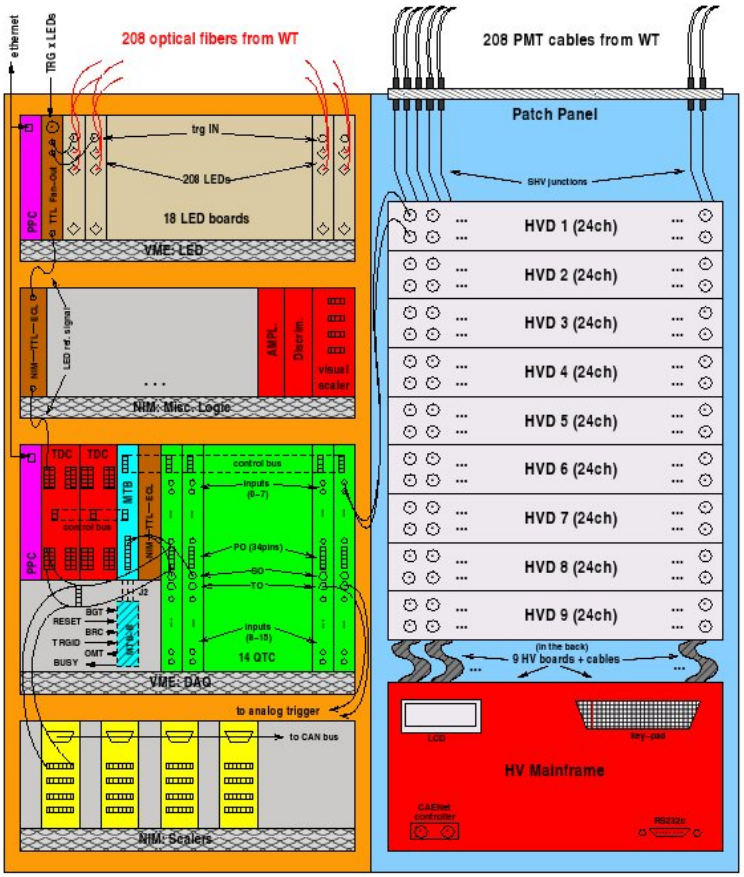

Figure 3.1: Schematic overview of the OD electronics hosted in two crates (orange and blue) [DDa06].

6. **TDC-boards**: These two time-to-digital-converters form the digital unit of the OD. It digitizes the incoming signals from the OTC-boards. Its memory buffer is periodically overwritten, until there is a stop signal related to the trigger. In this case, the memory is read out.

7. **LED-boards**: They are located at the top of the left rack. They are used for charge and time calibration of the PMTs, to which they are connected by optical fibers.

8. **PPC**: The two power PCs (pink colored) are needed to communicate with the VME-crates. For example, it allows to configure the MTB via remote.

3.2 The Pulser System in Detail

There was no possibility to check whether a zero rate shown in the scalers derives from a dead PMT or a dead QTC-channel. As part of this thesis, a system injecting a reference signal was designed, in anology to the one used for the Inner Detector. With the new installed pulser system the functionality of each single QTC-channel can be tested.

Fabrication
For means of simplicity the Pulser System was included to the HVD-boards. As base of

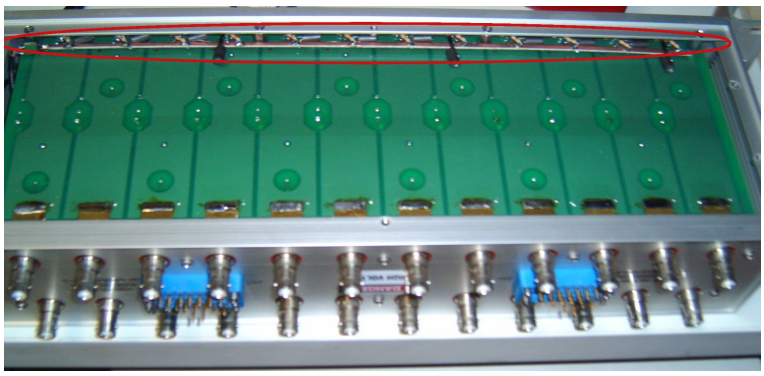

Figure 3.2: View into a HVD showing the integrated pusler sytem at the upper end of the board (marked in red).

the system, a copper bar (length $42cm$, depth $0.4cm$) was used (Figure 3.2). The bar was terminated with a resistor, considering that the total impedance must summarize to 50Ω. There were two possibilities to couple the pulser signal into each channel, via inductors or via capacitors. For comparison two different prototypes were built. They were assembled to the OD electronics system. The signal inducted was generated by a pulse shape generator. The output was compared via an oscilloscope regarding the shape of the output signal for the two cases. As there was only a little difference, it was decided to use the less expensive inductors. In total 11 HVD-boards (including two spare boards) had to be revised, each needing two of the prepared bars. Now the pulser system is coupled to the main DAQ system. If a pulser signal is issued, it is spread via two FAN IN/OUTS (Figure 3.3) to the 22 inlets of the system. It is important that the signal is applied to all channels simultaneously. A trigger is generated by the main DAQ and all channels are read out. The data can be used to identify the damaged channels. In the future it could also be used to test the relative time delays by the electronics of the individual channels. In each normal data run, the first 1000 events are used for detector calibration. Also pulser signals are present during these first events, to be able to identify damaged channels for each new run. During the further ongoing run, pulser signals are now injected in the OD- as well as in the ID-electronics at a rate of $0.1Hz$. With these pulser events it is possible to diagnose if a QTC-channel is not working correctly. If the injected pulser signal shows no damage in the QTC-boards but the channel shows no rate in normal events and scalers, the problem is connected to the PMT itself.

Working with the Pulser System
In Borexino, data handling and evaluation is the task of a single but very modular software called Echidna [DDa06]. The code is based on C++/root and stored on a central platform of the DAQ system. Everybody from the collaboration is able to download it to individual workstations even outside LNGS. Simultaneously uploads and downloads of new software developments are possible using *cvs*. In course of this thesis a evaluation program for the

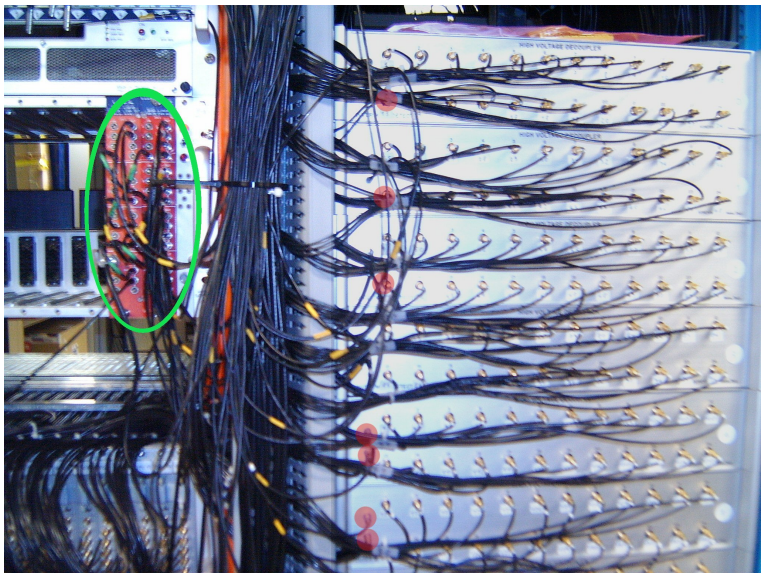

Figure 3.3: On the left side the two fan-outs can be seen (green). One the right crate the modified HVDs, with the new plug-ins for the pulser system (red), are mounted.

pulser system of the OD had to be implemented in Echidna. It was included in the framework of electronics-calibration modules. The new module, called *bx_calib_muon_pulser* can be activated in order to evaluate the functionality of the QTC-boards.
The module creates two histograms showing the injected pulser hits and the disfunctional QTC-channels. For the first one (Figure 3.4), pulser events are analysed for the individual pulser signals. If there is a signal present, the bin of the corresponding channel will be incremented. If the counts in a given bin is comparable to the number of events recorded, the corresponding channel is considered to be working. Channels showing zero or low rate are identified as disfunctional and are marked with an entry "1" on the second histogram (see Figure 3.5), working ones are marked "0". To show the temporal development of dead QTC-channels (getting damaged or repaired) exemplary runs have been evaluated. Table 3.1 shows this development, beginning 19.6.2007 and ending 29.9.2007. As it can

RunID	5300	5695	5752	6000
Date	19.6.2007	14.8.2007	21.8.2007	29.9.2007
Number of dead channels	1	3	5	0
Dead channel numbers	60	49, 51, 55	49, 51, 55 ,58, 62	

Table 3.1: Dead muon channels calculated with the module *bx_calib_muon_pulser*, using the pulser system. Time developement of nearly 3 month is covered.

be seen, it is importent to have a good surveillance of the status of the channels. A large number of missing channels can influence the significance of a measurement, as there are only relatively few PMTs (208) for the OD. Even a variance of 5 channels can disturb the muon track reconstruction and can effect the muon trigger efficiency.

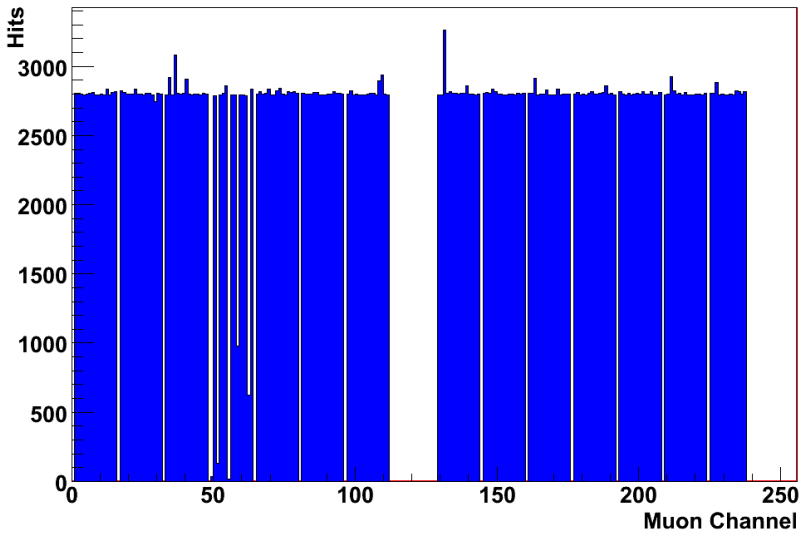

Figure 3.4: Events generated by the module *bx_calib_muon_pulser* using the injected pulser signals of Run5752. The periodical appearing gaps, every 16th channel, as well as the large gaps in the middle and at the end, are used as integrity channels. The broken QTC-channels 49, 51, 55, 58 and 62 show zero or largely diminished rate.

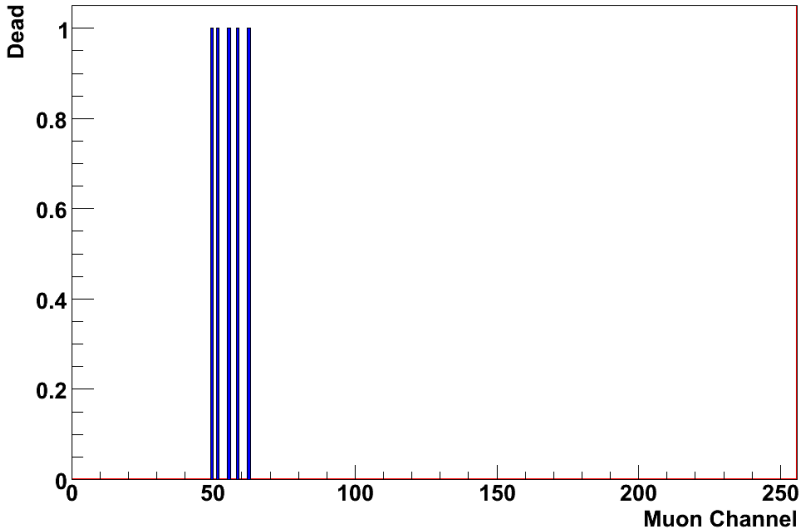

Figure 3.5: Dead QTC-channels 49, 51, 55, 58 and 62 in Run5752 as output histogram of the module *bx_calib_muon_pulser*.

The introduction of the pulser system enables a quick and easy check on dead channels. Therefore a rapid fix of the problem can be performed.

4 Simulation of the Outer Detector Electronics

Now, that Borexino takes real data, it is important to verify this data. The best possibility is to compare the measured data with simulations. Therefore, a program called g4Bx was invented. It is based on Geant4, and is able to simulate different particles interacting inside the detector. The dimensions, structures and materials of the total Borexino detector as well as their physical behaviour are implied in the code. It is possible to simulate a particle entering into the detector and producing Čerenkov light or scintillation. The so generated track can be calculated, just up to the point, the light would hit a PMT.
Now, another simulation program takes up. It is called bx_elec. Its code is written in C++. The program simulates the event, like a normal measurement would be processed with the Borexino electronics. So to speak to simulate the data arising from light, hitting a PMTs. Therefore all the electronic system of the detector, the PMTs, the frontend boards, the cables and so on, have to be considered in the program. The main task of bx_elec is to generate the so called hit data, that contains information about charge, time and place of the event. As input the simulated event of g4Bx is used. In addition the influence of the electronics itself on the data, like delay times and other offsets, has to be taken into account for the simulation. The output file generated has to be similar to the raw data file of a real run so that it can be processed with Echidna. The so obtained data is similar to the data of a normal run that has been processesed with Echidna. Therefore simulated and real events can be compared one-to-one.
At the beginning of this thesis bx_elec was just available for the inner part of the detector. Because it is also important to be able to check the data generated by the Outer Detector, the simulation program bx_elec was decided to be enlarged to the Outer Detector electronics. With this new part of the program it is possible to test an existing muon track reconstruction program. With the simulated data, knowing the muon's origin, track and energy the reconstructed path can easily be checked. Problems in the reconstruction program can be solved. Therefore the code of the electronics simulation program, bx_elec, was decided to be enlarged to the Outer Detector electronics. For that reason existing files had to be changed and new ones had to be generated. In this chapter the main changes and new invented parts for the simulation program bx_elec will be explained.
First, the two most important terms used in the following description are explained:

1. qtc_hit: It is a vector containing the hit information, time and charge. It is equal to the signals produced in the QTC-boards for a real run.

2. muon_hit: It is a vector containing the final hit information. It can be processed with Echidna, to generate a data sample equal to measured data. As input the qtc_hit vector is used.

The most important files that had to be reviewed are presented in Figure 4.1 along with their dependencies on each other. In total, 11 files had to be adapted, one had to be formed

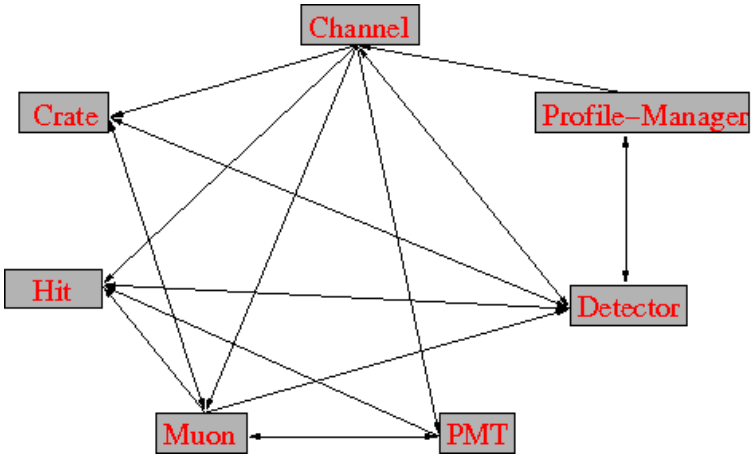

Figure 4.1: 7 Files of bx_elec with the most important changes. The arrows demonstrate the inter-file dependencies.

new. The most important are described in the following:

- **profile_manager**
  This part of the program is responsible for the alignment of the simulation with the real detector conditions. Therefore it reads the profile and the configuration saved in the Borexino database. The different data touples saved there, contain the information needed to adjust the simulation. For muons three different sections of the database had to be included:

  1. *MuonChannelSetting*: Here the info of the trigger status for each channel is stored. It can be seen if a channel was enabled during a run or not, and hence acquired data.
  2. *MuonChannelMapping*: This section provides information about the different channel types. There are three possibilities for each channel:
     - ordinary channel: normal data is acquired during a run
     - trigger channel: a trigger reference channel
     - laser channel: a LED reference channel for calibration purpose
  3. *HolesMapping*: Here information for channel identification is stored. The channels are allocated to holes, the PMTs are mounted in. Each hole has a unique set of coordinates, so each PMT position is exactly defined. This is very important for a later possible muon track reconstruction.

  The conditions of a specified run can now be reproduced. Therefore it is possible to compare the data obtained by simulation with real data.

- **pmt**
  This file is the most important one of the simulation program. It is responsible for

everything concerning the PMTs and generates most of the physikal data, especially the charge information. One of its main tasks is to store all photoelectrons detected by each single PMT. Therefore a vector is saved, containing a time ordering list of the recognized photoelectrons. This vector is needed to generate a hit that in reality is formed in the QTC-boards and therefore is called qtc_hit. It is compareable to the frontend_hit generated by the frontend-board of the Inner Detector electronics.
In addition all values needed to discribe a PMT's behaviour are set here. So for example the dark rate, the gain, charge raising time, used calibration charge for each PMT and many more. Also the decay times of the QTC-boards are set here. It will be used later on to determine if it is possible to separate two hits next to each other. As an output of this file, the charge deposited in the different PMTs is calculated and saved. There are three different types distinguished:

- normal charge: During a normal run the charge is calculated using information of the photoelectrons summed in the observed PMT
- calibration charge: The calibration pulse, generated by the LEDs, is used to calculate the calibration charge
- dark charge: If no hit and consequently no photoelectron is recognized by a PMT, the charge simulated is then similar to a dark rate of the PMT. It is generated by the dynode current and the thermoionic electrons of the photocathode in the respective PMT.

In this file also the qtc_hit is generated. As already mentioned it is similar to the frontend hit of the Inner Detector electronics. The main difference between inner and outer frontend hit is the calculation process of the charge. While for the inner detector, the charge is calculated via the hight of the produced peak (see Figure 4.2), the outer electronics frontend uses the length of a time window to calculate the charge

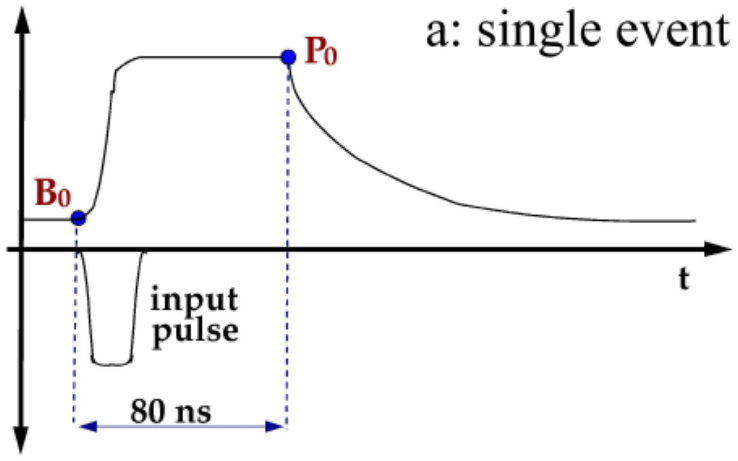

Figure 4.2: Charge calculation of the inner electronics using the base and peak of the spectrum [DDa06].

of a hit. This window is produced by the two values named trail-time and lead-time.

The lead-time is comparable to the start-time of a hit, the trail-time to the end-time. For charge calculation an offset produced by the QTC-chip has to be considered, too. This pedestal can be determined if no input signal is present during measurement. This is done during precalibrations of the Outer Detector at the startup of each normal run. A typical QTC-pedestal is $\sim 700ns$ (see Figure 4.3). The charge is then

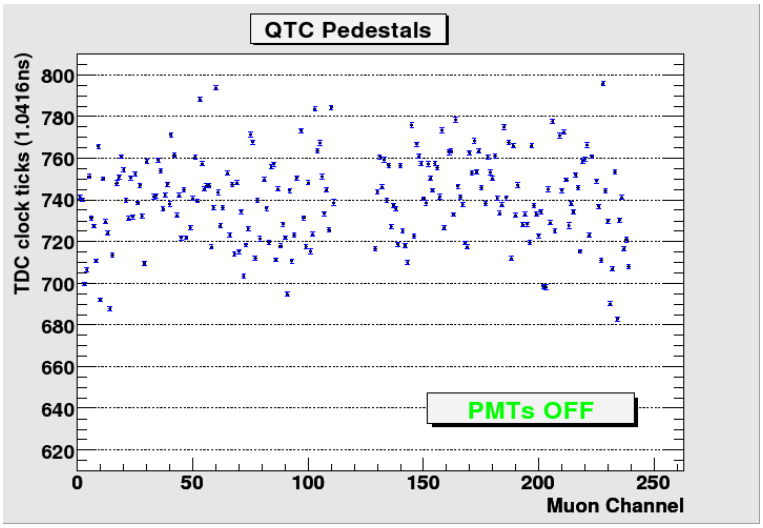

Figure 4.3: Pedestal of the QTC-chip [DDa06].

$$\text{charge} = [\text{trail-time} - \text{lead-time} - \text{pedestal}] \cdot \frac{1}{s}. \tag{4.1}$$

If two hits are too close in time, they can't be seperated. In order to determine if they can be seperated, a time value dt is introduced:

$$dt = \text{hit\_time} - \text{last\_hit\_time}. \tag{4.2}$$

If dt is too big compared to the delay time of the qtc-board, the ongoing hit is ignored and the next one is used. The obtained information of time and charge of a qtc_hit are saved, if the gtc_hit has no overlap with its previous one.

- **channel**
  First it is regarded which cannel is of ordinary type, what is set in the profile_manager. If it is ordinary, the channel is filled with dark noise. This and some other variables are declared and saved to the output file. So for exapmle starttime and endtime of the observed event. Also the photoelectrons registrated by the different PMTs are added to their associated channels.
  A section called MOUN CHANNELS was included to generate a so called muon hit. Therefore it uses information of the qtc_hit that is generated in the file pmt. Therefore the PMT has to be allocated as a muon PMT with a certain starttime and a logic channel number. After that all channels are reset and cleared, so that no previous hit informations are present. Then, if the PMT is triggered, a muon hit is generated

(see the file muon). If the amount of detected photoelectrons is over the threshold, defined in the file muon, it is declared as muon hit. Therefore every photoelectron coming from the PMT is summed. The muon hits are saved and stored to a vector called muon_hit_vector. For a better understanding, the dependancy of qtc_hit and muon_hit are illustrated in Figure 4.4.

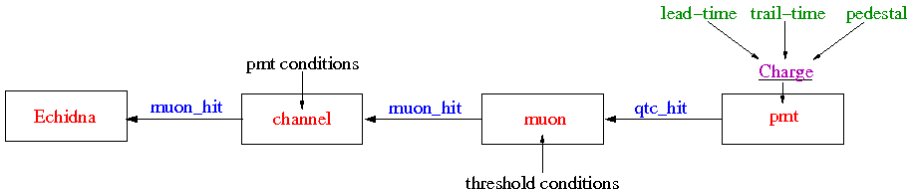

Figure 4.4: Schematic view of qtc_hit and muon_hit. The boxes represent the different modules. In blue the respective output is given. Black are different conditions needing to be fulfilled. Green is input data, the charge (magenta) is calculated with.

- **hit**
  Here values of the qtc-hits are set. Getters are defined to read the needed values out of the input file. As already mentioned, the main difference to the inner detector frontend boards is the charge information. The two variables lead_time and trail_time are defined and set here as well as the pedestal information of each channel. These are also variables used for the so called muon_hit. One of the important variables used is the logic channel_id (see file detector).

- **muon**
  This part of the simulation contains all parameters of a muon channel: Threshold, width of possible hits and different gate values. Data from the TDCs is collected, of capital importance the lead_time and trail_time. Then out of the qtc_hit the final muon_hit is formed and read by the file channel. It is regarded, if the hit accomplishes the threshold conditions for muons and if it satisfies time gate conditions. If it does, the muon_hit is built, saving the channel_id and charge information.

- **crate**
  A muon crate has to be imposed and a delay time is introduced, independent of the other crates of the Inner Detector. The different muon channels are assigned to this crate and enabled for further evaluation.

- **detector**
  This file is the core of the system. It combines all parts of the different files. The 216 muon channels are saved in a vector, arranging them in series to the 2240 inner channels. The muon channels then can be addressed using the logic channel numbers starting at 3001. Also the muon crate is saved to a vector, placed in series to the inner crates. The output contains information of the muon_hit. Also information of the experimental setup used during simulation are saved, e.g. how many channels were used in total, how many were dedicated to calibration or just contained darknoise.

The other files edited are mainly routines for exporting the parameters, so that every module and file can access them. The parser for the input file had to be changed, so that muon related data can be handled.
What is still missing is the reconfiguration of the trigger module. At the moment, the simulation is ment to use only the trigger of the Inner Detector. If there is a trigger, and therefore a hit in the inner electronics, the Outer Detector is fired and the outer electronics are read out. That means that untill now the electronics simulation for the Outer Detector can't be started separately of the one for the Inner Detector. For the future, it is planned to implement an independant trigger system also for the outer detector.

5 Response of the Inner Detector to Muon Signals

Borexino is built for measuring different neutrino fluxes. It is of great interest to keep the radioactive background as low as possible to get a clear neutrino signal. To guarantee this, great efforts have been made to keep the internal radioactivity as low as possible. The scintillator and the two vessels were treated with great care to satisfy the high requirements. Another problem is the cosmologic radiation. To prevent it, Borexino was built in an underground laboratory. Most of the radiation can be shielded, except for muons. These are the only particles, beside the neutrinos, being able to enter the laboratory from outside. They can interact in two different ways.

direct: Muons can hit the detector by themselves. They have two different possibilities travelling throug the detector

- First, they can pass through the Inner Vessel. They will generate so much scintillation light in the scintillator, that their visible energy is much higher than that of neutrinos. Therefore, it is no problem to distinguish them from neutrinos.
- Second they can only hit the buffer. Čerenkov light emission is generated with an asymmetric light output. But as the Inner Vessel scintillator can be excited, this energy is compareable to the one generated by neutrinos. Hence, problems in distinguishing them from neutrinos occur.

indirect: They can interact with the surrounding rock or air and produce spallation products, which also can enter the detector. For that reason the OD has been built. First, it is an additional shielding against radiation present in the laboratory. Second, muons can be detected and labled as that. Therefore even spallation products of muons can be allocated. In Chapter 6 the efficiency of the Outer Muon Veto will be discussed in more detail. But it is not the only possibility to distinguish between neutrino-like and muon-like. In course of this thesis, possibilities were investigated to discriminate them using the response of the inner detector. Especially the fact that neutrinos interact point-like whereas muons are track events offer possibilities to discriminate them. This and other options will be explained in this chapter.

The data, used for evaluation, covers the runs starting from Run5500 and ending at Run5657. Some of the data couldn't be used as the Outer Muon Veto or the Inner Detector was not working correctly, see Table 5.1. The remaining data adds to a total run time of about 14 days.
As the energy threshold of Borexino is about $200keV$ it only makes sense to regard events with higher energies. The analysis is devided into several energy regions including the mentioned neutrinos:

RunID	5517	5559	5600	5602	5617	5639	5643	5650
ID Rate	55.5	133.3	142.5	315.7	122.5	131.3	2.9	391.6
OD Rate	169.5	427.3	343.8	453.4	320.0	0.0	20.2	433.7

Table 5.1: Runs rejected for evaluation. For a normally working detector the values would arise to a rate of approximately 180 for the Inner Detector and approximately 450 for the Outer Detector.

1. $200keV$ — $800keV$: ^7Be neutrinos
2. $0,8MeV$ — $2MeV$: pep, CNO neutrinos
3. $2MeV$ — $5MeV$: ^8B neutrinos
4. $5MeV$ — $10MeV$ ^8B neutrinos
5. $10MeV$ — ∞ ^8B neutrinos

It is possible for muons to be present in all energy regions. If they interact with the surrounding rock they can lose a lot of energy. That means that their remaining energy is decreasing.
The last energy sector has another important role. For this high energies it is very unlikely that there are any existing neutrinos. The expected neutrino rate is getting low and background radiation vanishes. If in this region any other than muolike events are identified it can be a hint of an inefficiency of the Outer Detector (see Section 6.2). There are three different units for energy provided by Echidna: *charge*, *hits* and *npe*. *Charge* is the charge that is deposited in a PMT. The number of recorded hits in a single PMT is given by *hits*. Last, *npe* gives the number of photoelectrons recognized by one PMT. All the three units can be transformed into energy. The one used here is *charge*. The conversion factor is

$$500\ charge \approx 1MeV. \tag{5.1}$$

5.1 Deutsch-Parameter

As already mentioned in Chapter 2 the Inner Detector is equipped with two different kinds of PMTs. The majority has light concentrators. This reflective aluminum cone collects the light coming from the front and focusses it on the photo cathode. The field of view is focussed on the fiducial volume, what enhances the light yield for events in the Inner Vessel but narrows the acceptence angle. These PMTs are nearly blind for events in the buffer region. On the other hand there are the 374 PMTs without light-concentrators. They have a larger field of view because of their not narrowed acceptance angle. This difference in relative light yield in the two subgroups of PMTs for Buffer and Inner Vessel events makes it possible to use the PMTs of the Inner Detector as a Muon Veto.
The relative light yield of muon tracks outside the Inner Vessel and point-like source in the Inner Vessel will be different as regarding the charge, deposited in the different PMTs. The fraction

$$D = 1 - \frac{charge\ of\ PMTs\ with\ concentrators}{total\ charge\ of\ all\ PMTs} \tag{5.2}$$

is higher for muons than for neutrinos. The parameter D is called Deutsch-Parameter. It is named after Martin Deutsch, who developed the concept of this veto technique together with Lothar Oberauer.

Regarding events of the Inner Detector, the Outer Detector was used to distinguish between neutrino-like and muon-like events. Whenever the Outer Detector was triggered the event in the Inner Detector was marked as a muon-like event otherwise as a neutrino-like event. The events shown in red (Figure 5.1) are neutrino-like, the ones in blue muon-like. The Deutsch-Parameter is plotted in dependance on the charge. The plot covers the whole

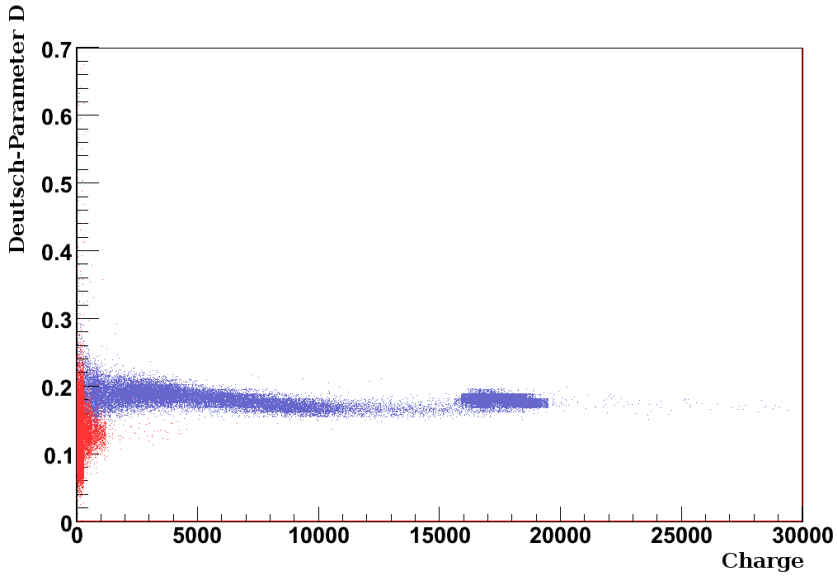

Figure 5.1: Deutsch-Parameter for the total energy spectrum of events detected in Borexino. The two colours distinguish between neutrino-like (red) and muon-like (blue) events.

energy range of events observed in Borexino. As the Outer Muon Veto is able to identify a large fraction of the muon-like events, it can be seen that neutrino-like and muon-like events distribute around different mean values. Therefore they can be seperated by introducing a fixed cut parameter, the Deutsch-Parameter. The efficiency of this cut is plotted in Figure 5.2. Again red colour is used for neutrino-like and blue for muon-like events. For a better graphical demonstration, the y-axis shows the chance of a miss-identification of muon-like and neutrino-like events. For the 0 limit of the cut everything is identified as muon. For higher cut values, the situation changes, more and more neutrino-like events are identified rightly untill no efficiency for muon identification is left. Everything is then regarded as a neutrino. The best balanced cut for both, is the crossing point of the red and blue function. Especially for high energies a separation of the two distributions can be observed. A detailed view of the different energy scales is shown in Figure 5.3. Up to an energy of about $1MeV$ the distribution of neutrino-like and muon-like events have a larger overlap region. This makes a meaningful discrimination more difficult. For energies above $10MeV$ there are only few neutrino-like events left. For better visibility they are emphasized in the plot.

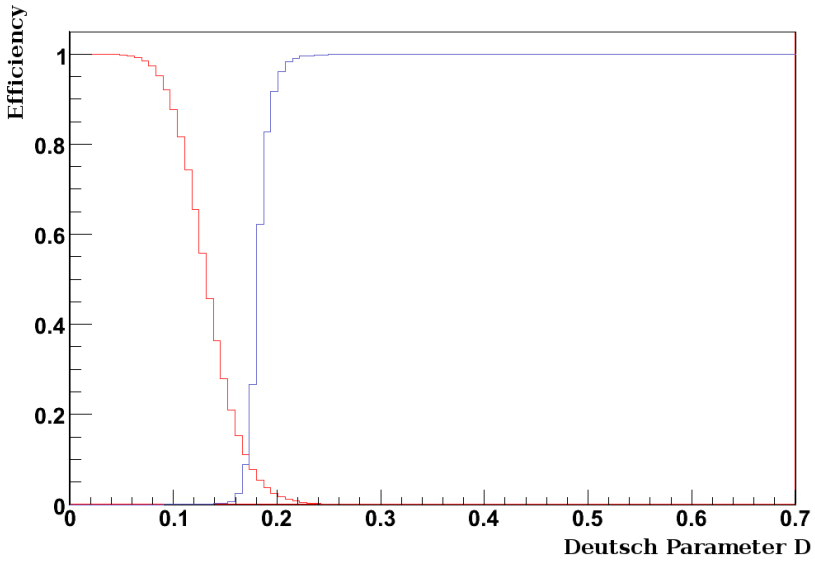

Figure 5.2: Efficiency of the Deutsch-Parameter cut for the total energy range. Neutrino-like events shown in red and muon-like in blue. All particles identified correctly equals 0. All particles detected as the other ones equals 1.

Events lying within the distribtion of muon-like events give a hint for the inefficiency of the Outer Muon Veto that will be discussed in Chapter 6.
The efficiencies of the Deutsch-Parameter cuts for the different energy ranges (Figure 5.4), whereas neutrino-like and muon-like events have the same identification possibility, are summarized in Table 5.2. Of course the cut depends on the purpose of the user. If one pays

Energy $[MeV]$	$200-800$	$0.8-2$	$2-5$	$5-10$	$10-\infty$	$0-\infty$
Deutsch-Parameter	0.160	0.159	0.161	0.175	0.177	0.173
Efficiency [%]	82	93	98	94	60	90

Table 5.2: Best values for the Deutsch-Parameter cut. Both, neutrinos and muons have the same efficiency at that point. The efficiency here gives the percentage of detecting a particle as what it is.

more attention to identify all muons, the cut must be lowered. Raised, if more neutrinos should be identified.

5.2 Meantime vs. Peaktime

Another possible cut can be performed by the mean time. The mean time is the mean value of the time period of each hit relative to the start-time of the first hit. Neutrinos, detected due to scintillation in the Inner Vessel, produce a fast excitation of the liquid scintillator, comparable to light travel times. In general their mean time last up to $100ns$. Muons are

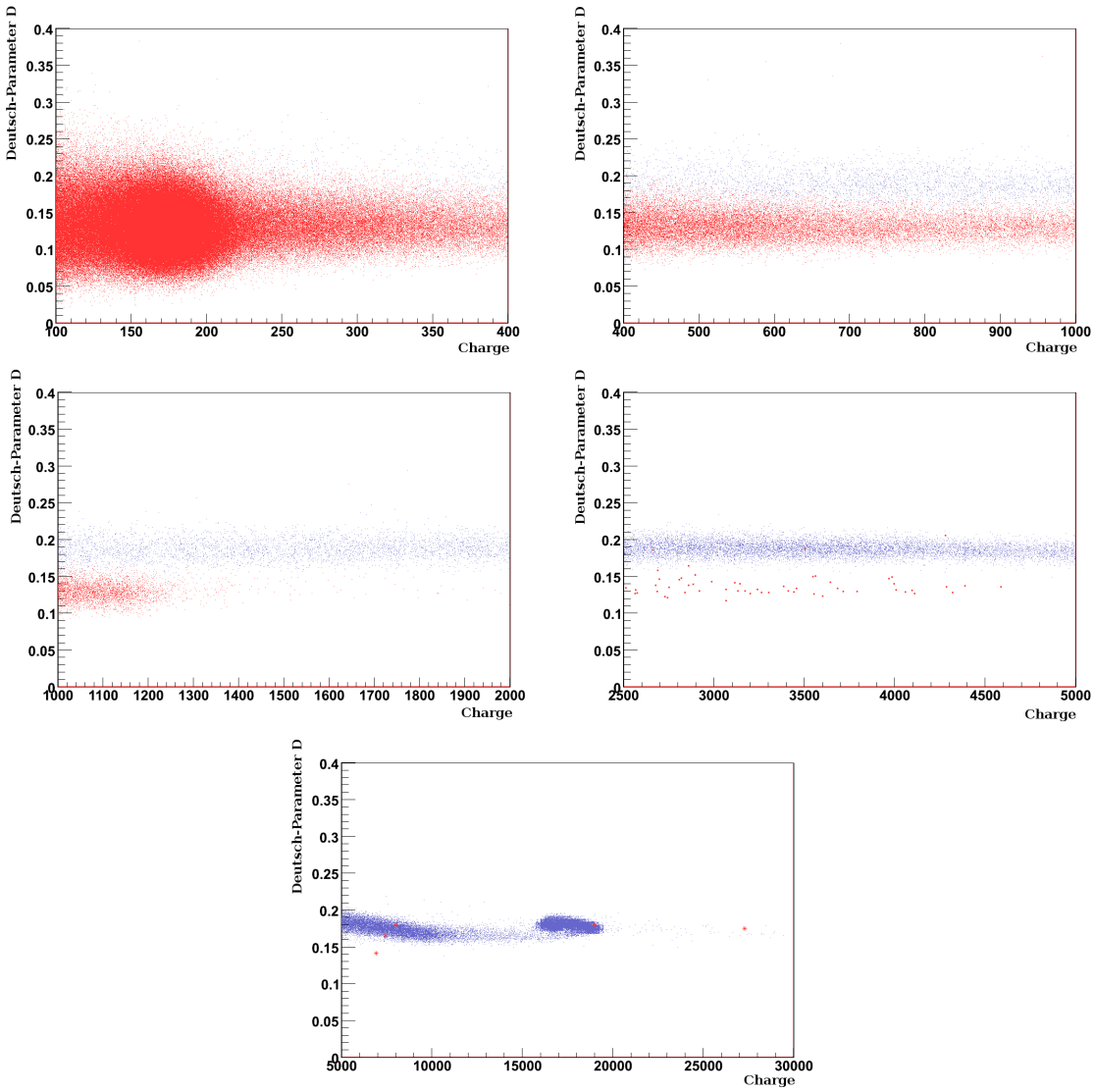

Figure 5.3: Deutsch-Parameter for the different energy ranges as described in Chapter 5. Separation of neutrino-like (red) and muon-like (blue) events.

different in their behaviour. They produce Čerenkov light in the buffer. It is much less light generated along the track and has a broader distribution. Their mean time can last up to $3000ns$. Low energetic muons can have short tracks and therefore behave more as point-like particles as high energetic muons. Hence, there might be problems for low energy areas, to distinguish between neutrino-like and muon-like events. Therefore an other parameter is used as cut in addition to the mean time, the peak time.
The peak time is the time of the light emission peak relative to the beginning of the pulse. This time is short for the point-like interacting neutrinos. For muons travelling through the detector, creating Čerenkov light, the pulse will rise slowly in intensity. That will result

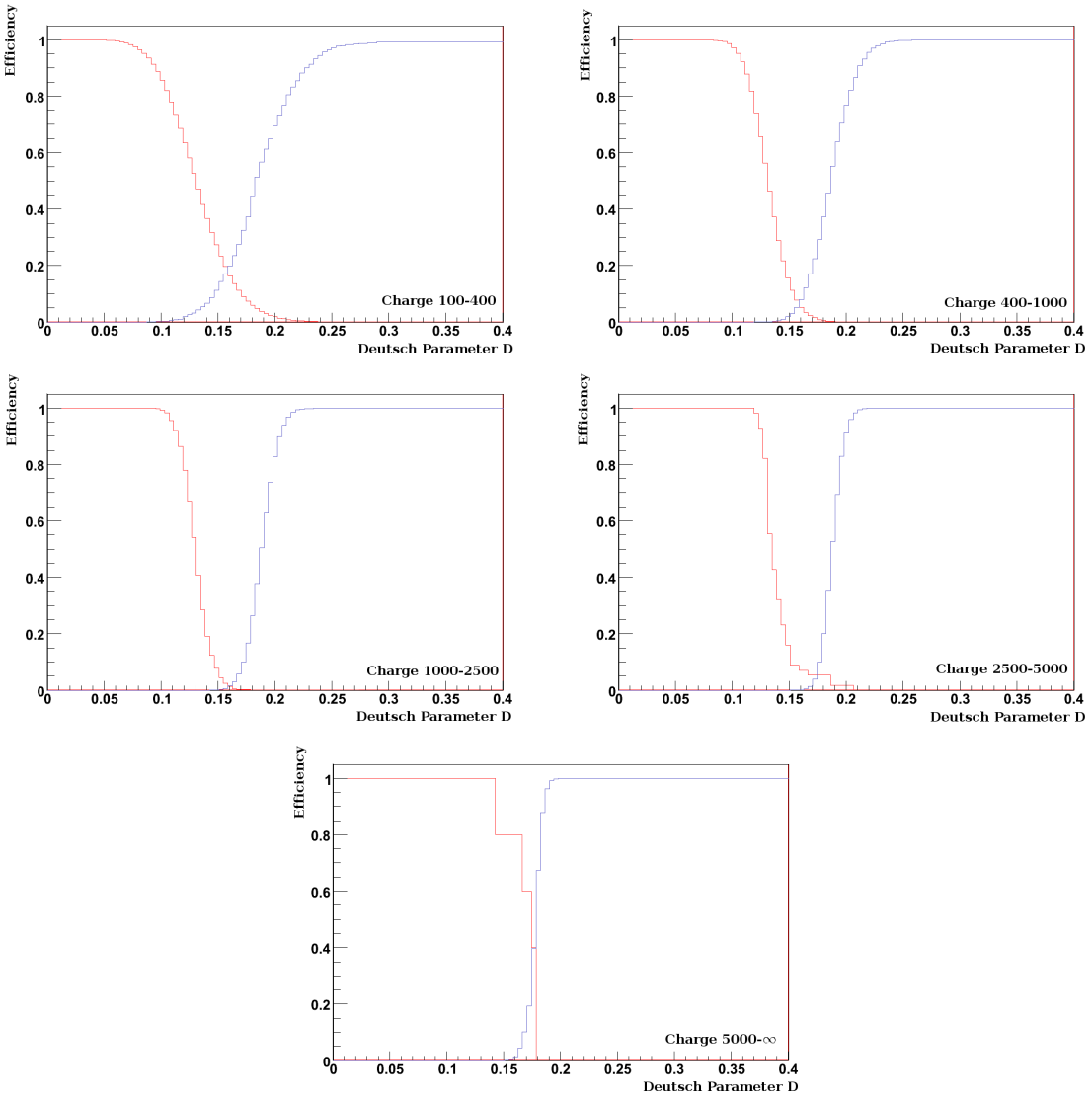

Figure 5.4: Efficiency of the Deutsch-Parameter cut for the different energy scopes. It is the chance for miss-identification. Neutrino-like events shown in red and muon-like in blue.

in a long peak time. To illustrate the described differences in the mean and peak time a shematic energy spectra is plotted for neutrino-like and muon-like events (Figure 5.5).

Combining both the mean time and the peak time a good distinction between neutrino-like and muon-like events can be performed. In Figure 5.6 the peak time is plotted versus the mean time for the total energy range. Again, the Outer Detector was used to identify neutrino-like (red) and muon-like (blue) events. As it can be seen there are some disturbing events with a very low peak time covering almost the total range of mean times. Most

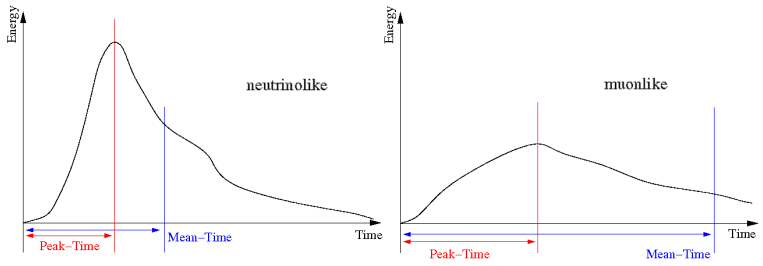

Figure 5.5: Schematic spectra showing mean time and peak time for neutrino-like and muon-like events.

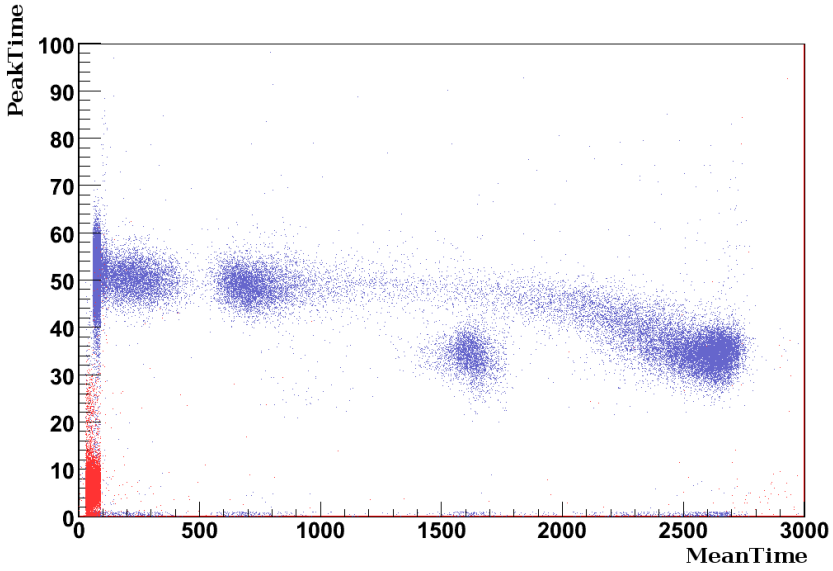

Figure 5.6: Peak time versus mean time. Both units are given in ns. Neutrinos shown in red and muons in blue.

of them are flagged as muons. The events are distributed evenly over all runs. A combination with a fiducial volume cut (Section 5.5) will not remove them. It seems that they are physical events. Due to these events the possibility to set a cut is affected. In further analysis the peak time is used as cut parameter. It was also tried to use a combination of mean time and peak time as cut parameter, but the efficiency, especially for low mean and peak times, didn't improve. The cut for the total energy range is shown in Figure 5.7. Like in the previous section the efficiency plotted is for miss-identifying the respective particle. That means, for low peak time cuts nearly all particles are identified as muons while for high values everything is identified as neutrino.
The different energy windows are gathered in Figure 5.8. Because of the above mentioned problem the peak time cuts for all energy windows are disturbed slightly (see Figure 5.9).
The best balanced cuts for muon-like and neutrino-like events are summarizied (Table 5.3). It can be seen, that for higher energies (above $2MeV$), the cut parameter has higher values. That is in compliance with the expectations. High energetic muons travelling through the

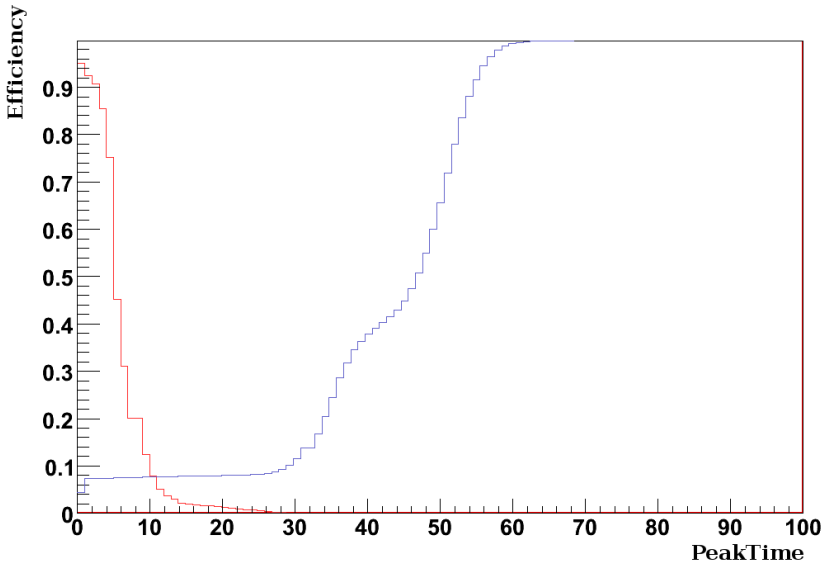

Figure 5.7: Efficiency of the peak time cut. Netrino-like events shown in red muon-like in blue. All particles identified correctly equals 0. All particles detected as the other ones equals 1.

Energy $[MeV]$	$0.2-0.8$	$0.8-2$	$2-5$	$5-10$	$10-\infty$	$0-\infty$
Peak time $[ns]$	8.1	14.5	13.5	19.3	35.2	10.5
Efficiency [%]	84	93	92	92	65	92

Table 5.3: Best values for the peak time cut. Both, neutrino-like and muon-like events have the same efficiency at that point. The efficiency here is the chance for miss-identification

detector generate more Čerenkov light and a longer track and therefore the peak time rises.

5.3 Tail-to-Total

As a third method the so called Tail-to-Total method can be used. Normaly this method is used to do α/β-discrimination, as α-signals decay more slowly than β-like events due to the properties of ionization in the liquid scintillator. Tail-to-Total uses the ratio of the area of the signals "tail" to the total area. These areas are formed by pulse integrals. For this purpose the deposited charge is saved in a $100ns$ wide window. The window is then devided into another window starting from $15ns$ untill the end. It therefore can be called tail-window in comparison to the total-window. The ratio of the integrated charge pulses, so to speak the ratio of the pulse integrals of the tail-window and the total-window, makes it able to discriminate α- against β-particles. To test that this discrimination is working properly, it was used to the ^{214}Bi-^{214}Po decay coincidence, present in the ^{220}Rn decay chain, and was affirmed (Figure 5.10). The two distributions for α- and β-particles are

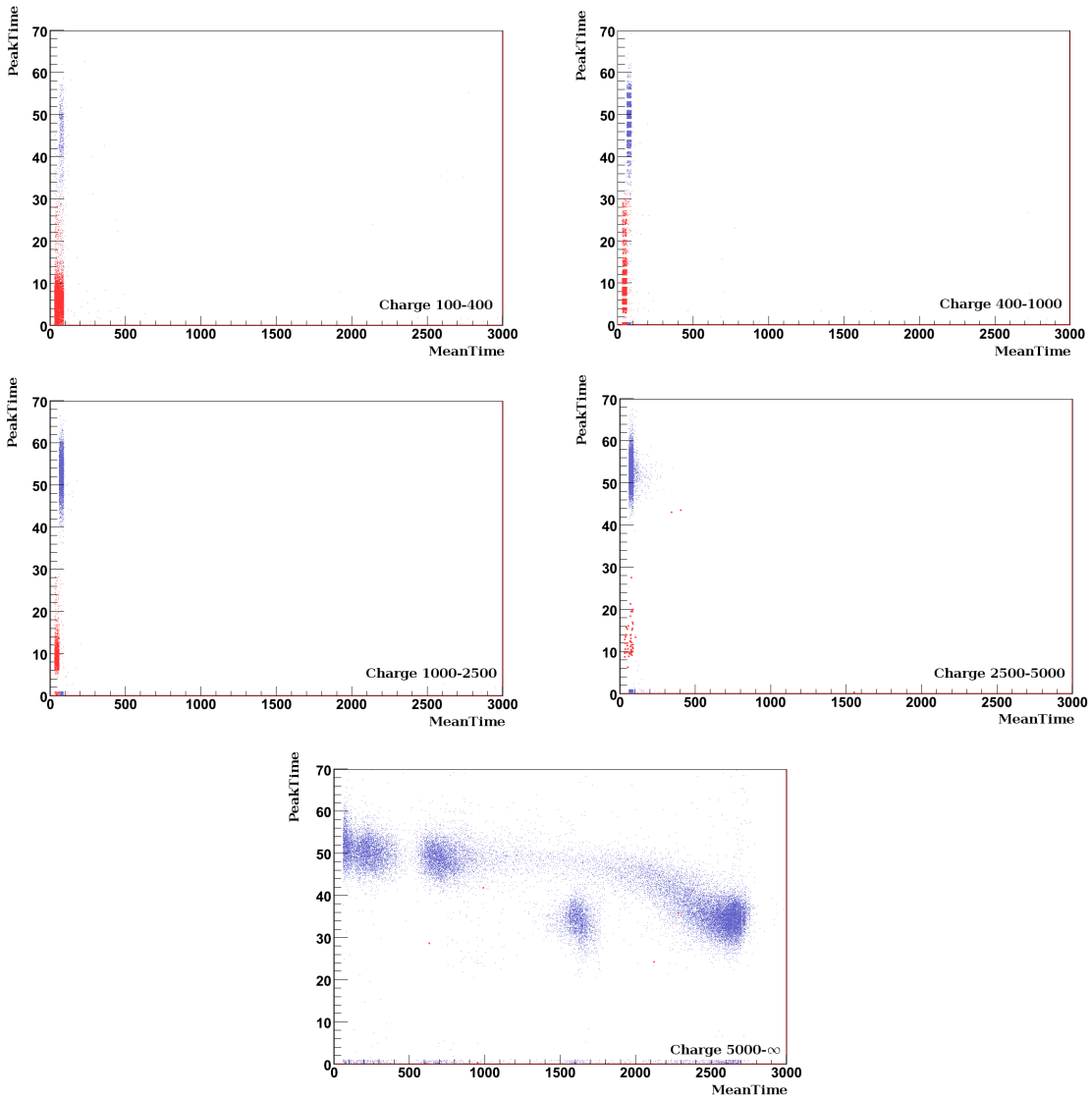

Figure 5.8: Peak time versus mean time for the energy windows defined in Chapter 5. Separation of neutrino-like (red) and muon-like (blue) events.

clearly separated, but still have an overlap, what implies some uncertainties. In general β's gather around a smaller Tail-to-Total ratio as the α's.

It is possible to use this ratio to discriminate neutrino-like against muon-like events. It is expected that neutrinos behave more like β-particles due to their point-like interaktion with electrons. The ratio of the time windows is supposed to remain small. For muons it is different. Because of their long track through the inner detector, the deposited charge rises slowly, and don't form a peak before the end of the $100ns$ time gate. Therefore their Tail-to-Total value is relatively high. In that way, muons can be identified along with the

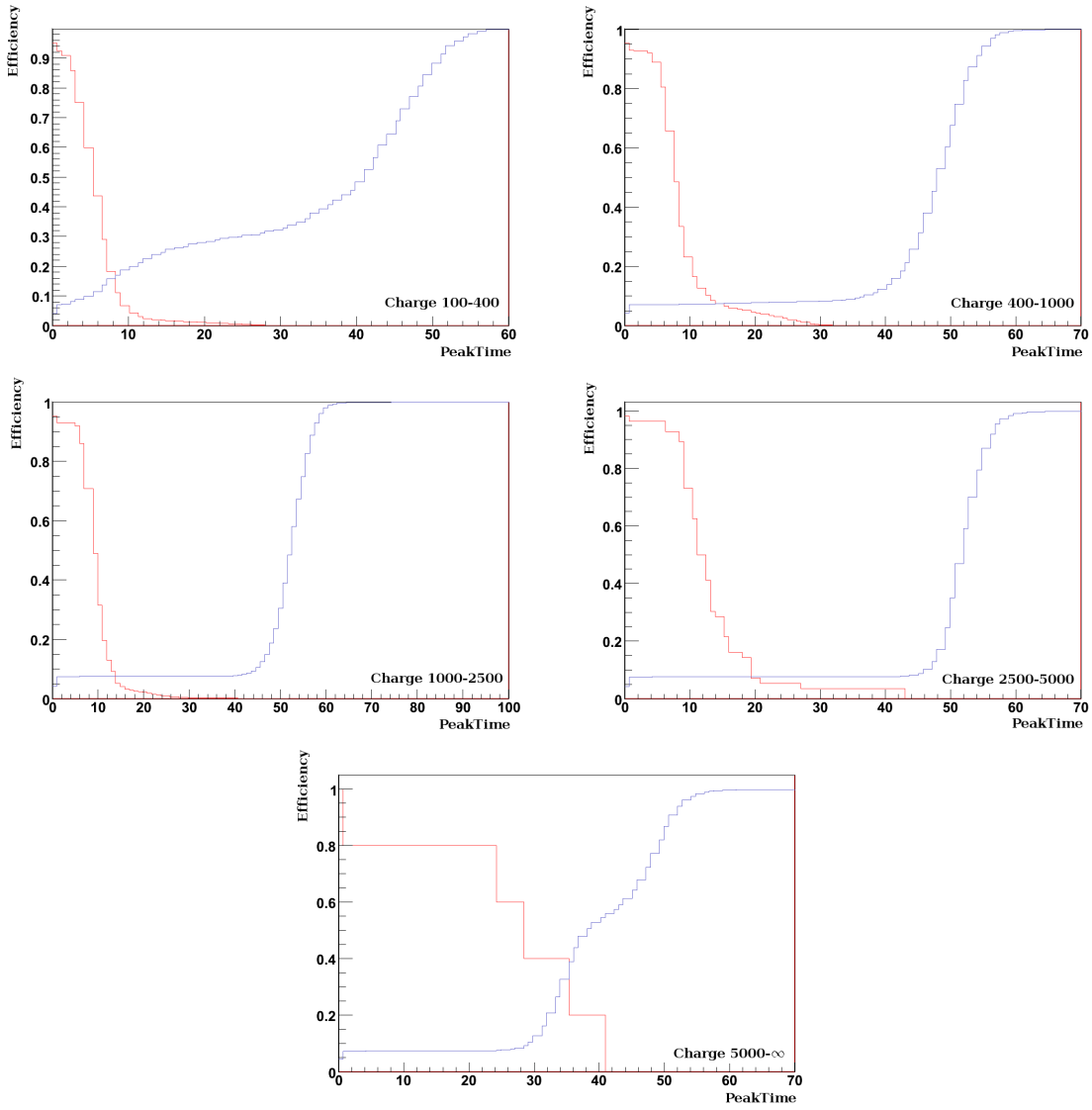

Figure 5.9: Efficiency of the peak time cut for the energy windows defined in Chapter 5. Separation of neutrino-like (red) and muon-like (blue) events. All particles identified rightly equals 0. All particles identified as the other ones equals 1.

α-particles using the Tail-to-Total method.
Using this method to distinguish between neutrinos and muons, one expects a clear separation of them. The neutrinos will be distributed around a small value, while the mouns will obtain higher values. Regarding the Tail-to-Total ratio for the total energy range (Figure 5.11), this assumption can be certified. Using the Outer Detector, particles identified as neutrino-like events are displayed in red in the plot, muon-like events in blue. The efficiency for miss-identification of a muon or a neutrino is shown in Figure 5.12. The relatively poor efficiency, compared to the Deutsch-Parameter, can be explained by the following. Espe-

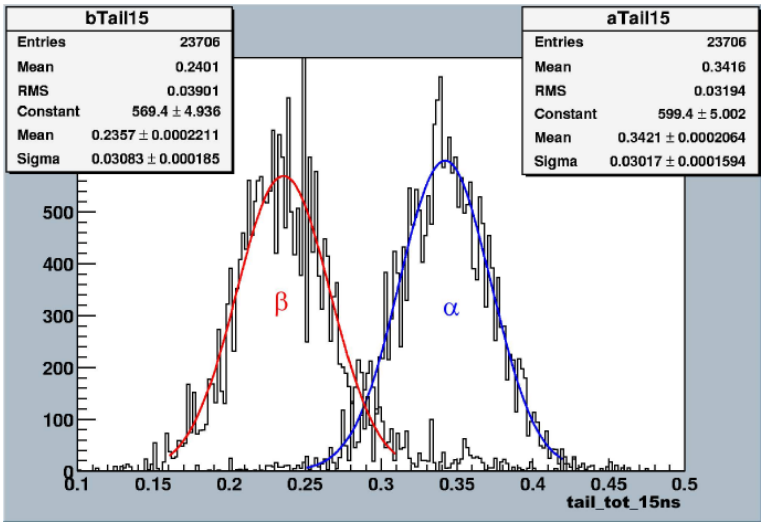

Figure 5.10: α/β separation with the Tail-to-Total method for the ^{214}Bi-^{214}Po decay coincidence of the AR8 source run [DDa06].

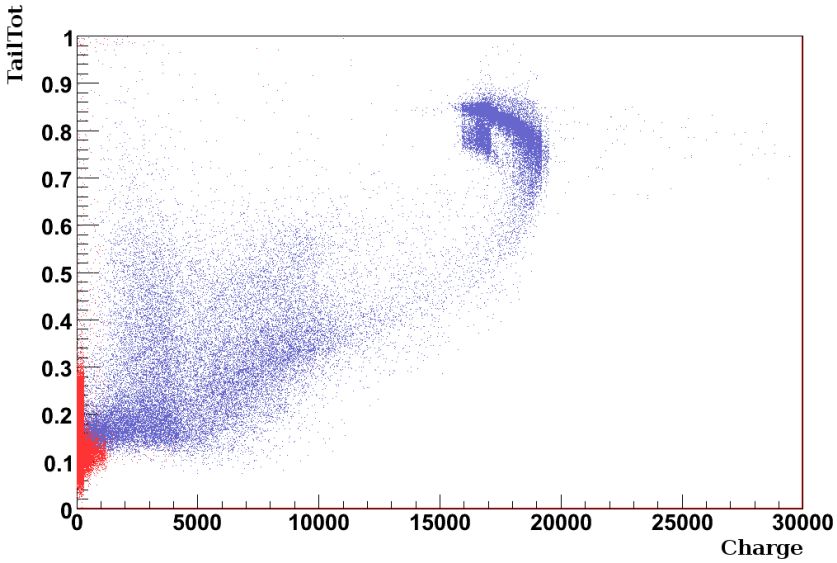

Figure 5.11: Tail-to-Total value for the total measured energy spectrum. Neutrino-like events shown in red and muon-like in blue. A separation, like for α- and β-particles, can be observed.

cially for the low energy range, the sample of neutrino-like events is disturbed by a lot of α-particals, due to the ^{210}Po peak as already mentioned in Chapter 2.2. For higher energy ranges these disturbing α-particles vanish, and the identification will increase. This can be seen regarding the different energy windows (Figure 5.13) and the associated efficiencies of miss-identifying particles (Figure 5.14). An other point that can affect the identification,

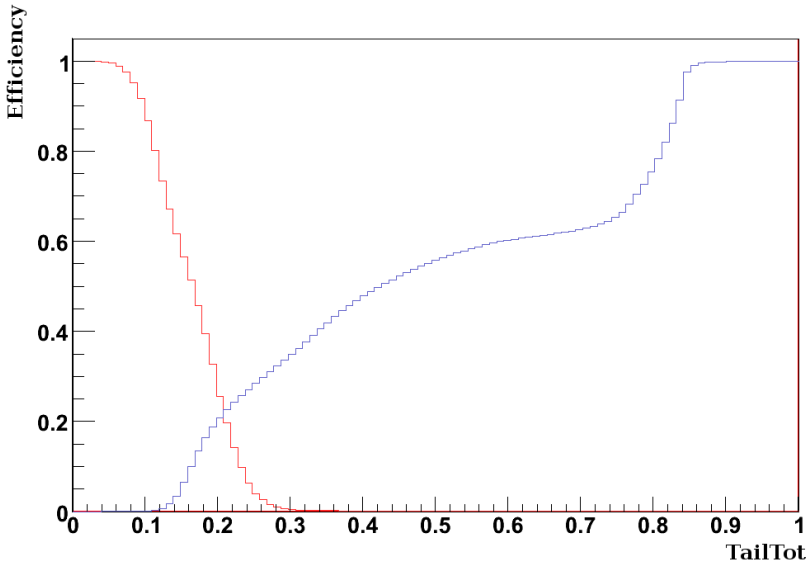

Figure 5.12: Efficiency of the Tail-to-Total method for the total energy range. Neutrinos shown in red and muons in blue. All particles identified correctly equals 0. All particles detected as the other ones equals 1.

is that even for α- and β-particles the different Tail-to-Total ratios have an overlap. Therefore, with a certain plausibility, β's can be identified as α's and vice versa.
For the last energy window, $5MeV - \infty$, there is only low probability for neutrinos. That influences the efficiency enormously.
The best cut parameters, where neutrino-like and muon-like events have the same efficiency, are collected in Table 5.4. It can be seen that most of the cut parameters have a similar

Energy $[MeV]$	$0.2-0.8$	$0.8-2$	$2-5$	$5-10$	$10-\infty$	$0-\infty$
Tail-to-Total	0.165	0.145	0.150	0.159	0.775	0.210
Efficiency [%]	44	85	93	89	44	79

Table 5.4: Best values for the Tail-to-Total cut. Both, neutrino-like and muon-like events have the same efficiency at that point. The efficiency here is the percentage of identifying a particle correctly.

value for separating α's and β's. This confirms the possibility to treat neutrinos and muons with the Tail-to-Total method and to use it as a possible separation cut.

5.4 Likelihood

There are three codes (Milan, Dubna and Moscow) that are doing position reconstruction. Their aim is to determine the exact position of point-like events in the Inner Detector. They are optimized for reconstruction in the Inner Vessel. The three codes were developed

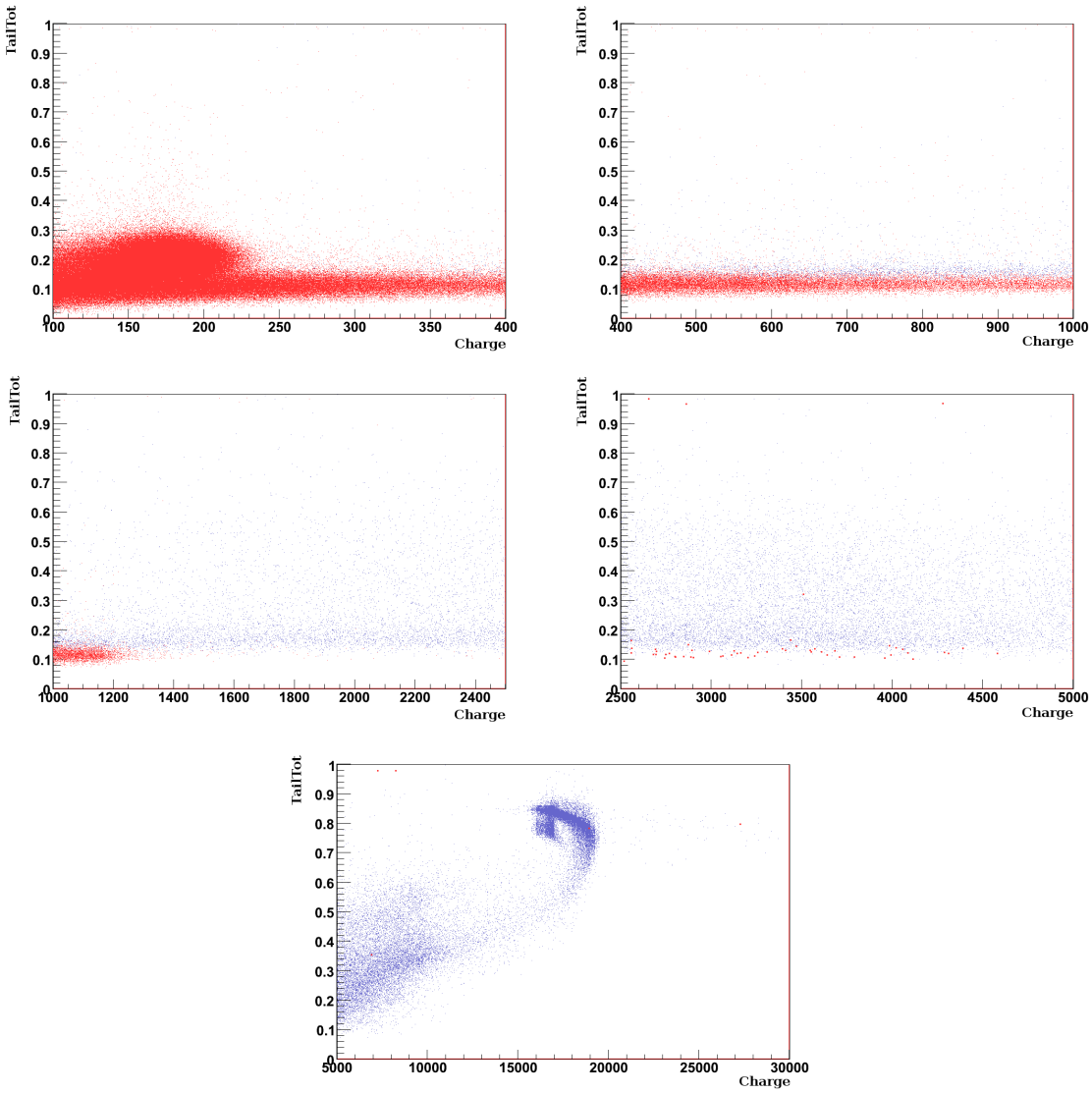

Figure 5.13: Tail-to-Total value for different energy windows. Neutrinos shown in red and muons in blue. A separation, like for α- and β-particles, can be observed.

independently from each other, which allows to compare the results. At the moment, the Milan code is used by most members of the collaboration. Because of the point-like behaviour of neutrinos their reconstruction should be an exact point. As a benchmark for the quality of this reconstruction the parameter likelihood was invented and is stored along with the reconstruction position. A low likelihood accords to a good point-like reconstruction. Muons of course are no point-like sources as they emit Čerenkov light all along their flight path. Therefore a reconstruction of the reaction point is not very meaningful. If it is performed anyhow the quality of the point-like reconstruction will be low. That should also be reflected in the likelihood parameter.

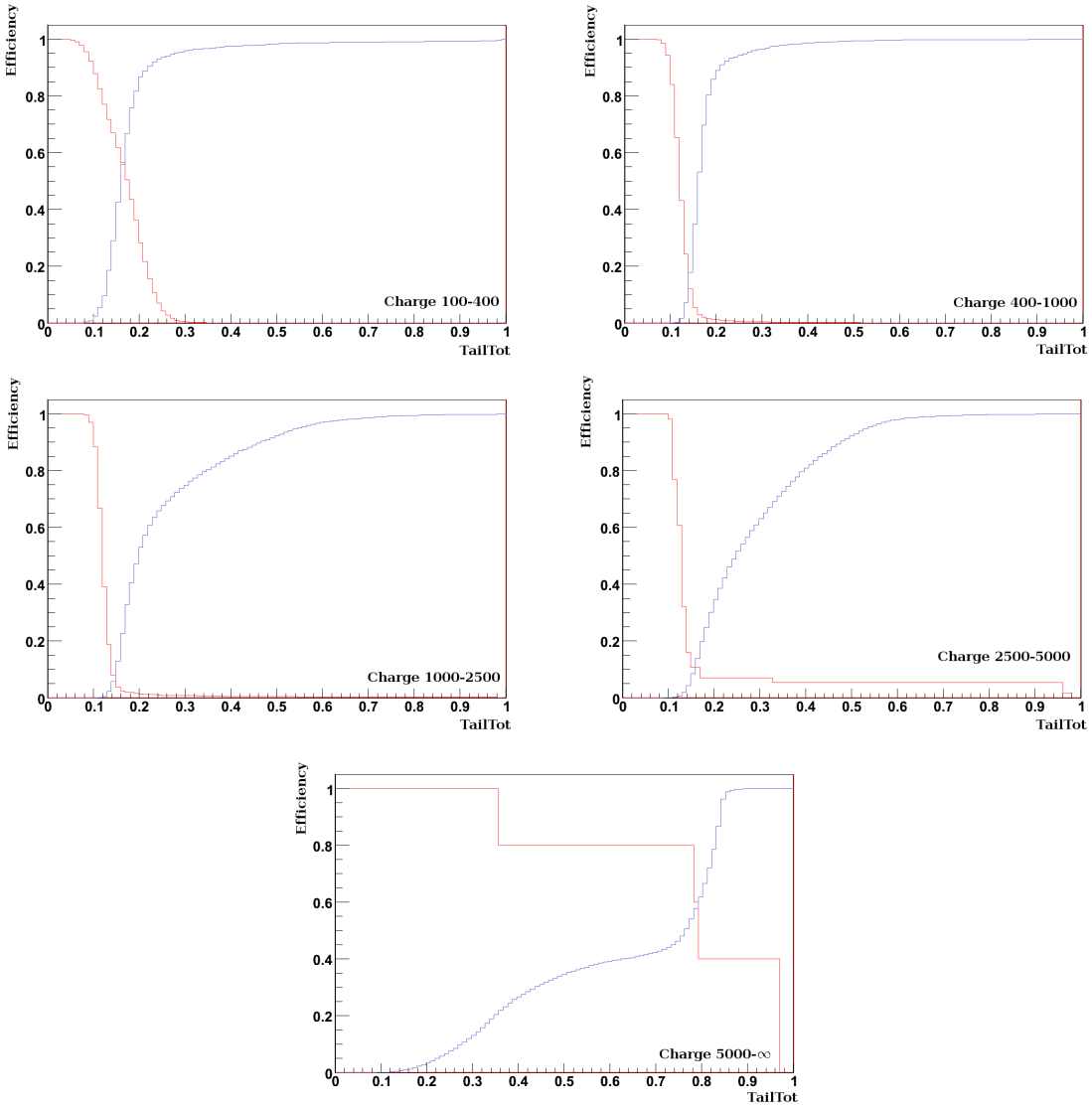

Figure 5.14: Efficiency of the Tail-to-Total method for different energy windows. Neutrinos shown in red and muons in blue. All particles detected as themselves equals 0. All particles detected as the other ones equals 1.

The reconstruction code used for this analysis, was the one developed by the Milan group. The spectrum in Figure 5.15 shows this parameter for the total energy range detected in Borexino. The particles identified by the Outer Muon Veto as neutrinos are shown in red, the ones detected as muons in blue. A seperation between neutrinos and muons can be performed using the quality of the reconstruction, the likelihood, as cut parameter. The efficiency for this cut is shown in Figure 5.16. Regarding the different energy areas (Figure 5.17) and their efficiencies (Figure 5.18) one can see that this cut, compared to the other ones described in the sections before, is very powerful. Especially in the energy range from

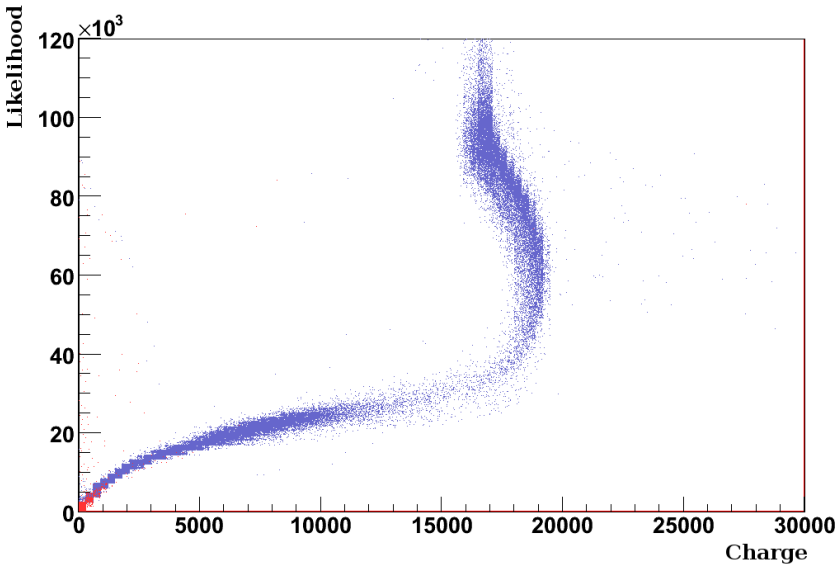

Figure 5.15: Likelihood parameter for the total measured energy range. Neutrino-like events shown in red and muon-like in blue. A low likelihood reflects a good event reconstruction, a large one a bad reconstruction.

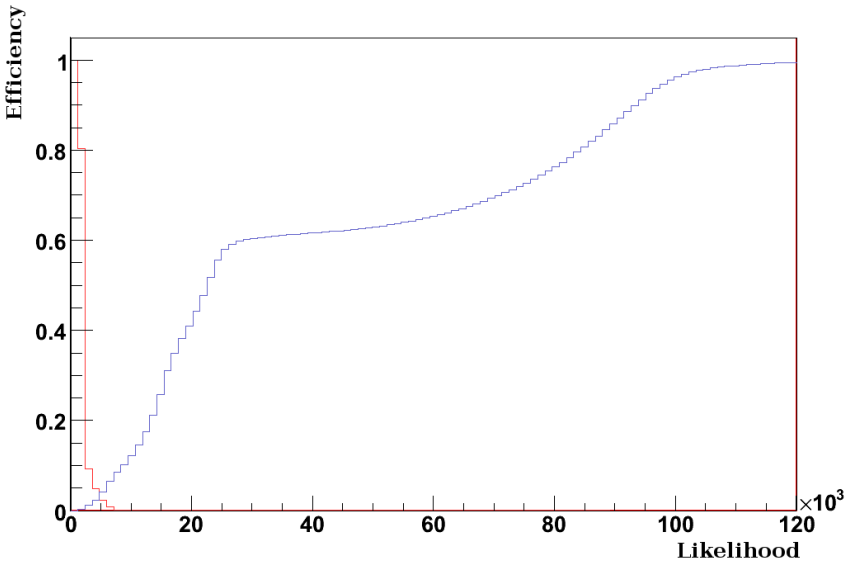

Figure 5.16: Efficiency of the likelihood cut for the total energy range. Neutrinos shown in red and muons in blue. All particles identified correctly equals 0. All particles identified as the other ones equals 1.

$2MeV$ to $5MeV$, the ^8B neutrino window, this cut can play an important role to distinguish between neutrinos and muons. It is also the best cut regarding the total energy spectrum. The imprecision of the neutrino efficiency in the last energy range can again be explained

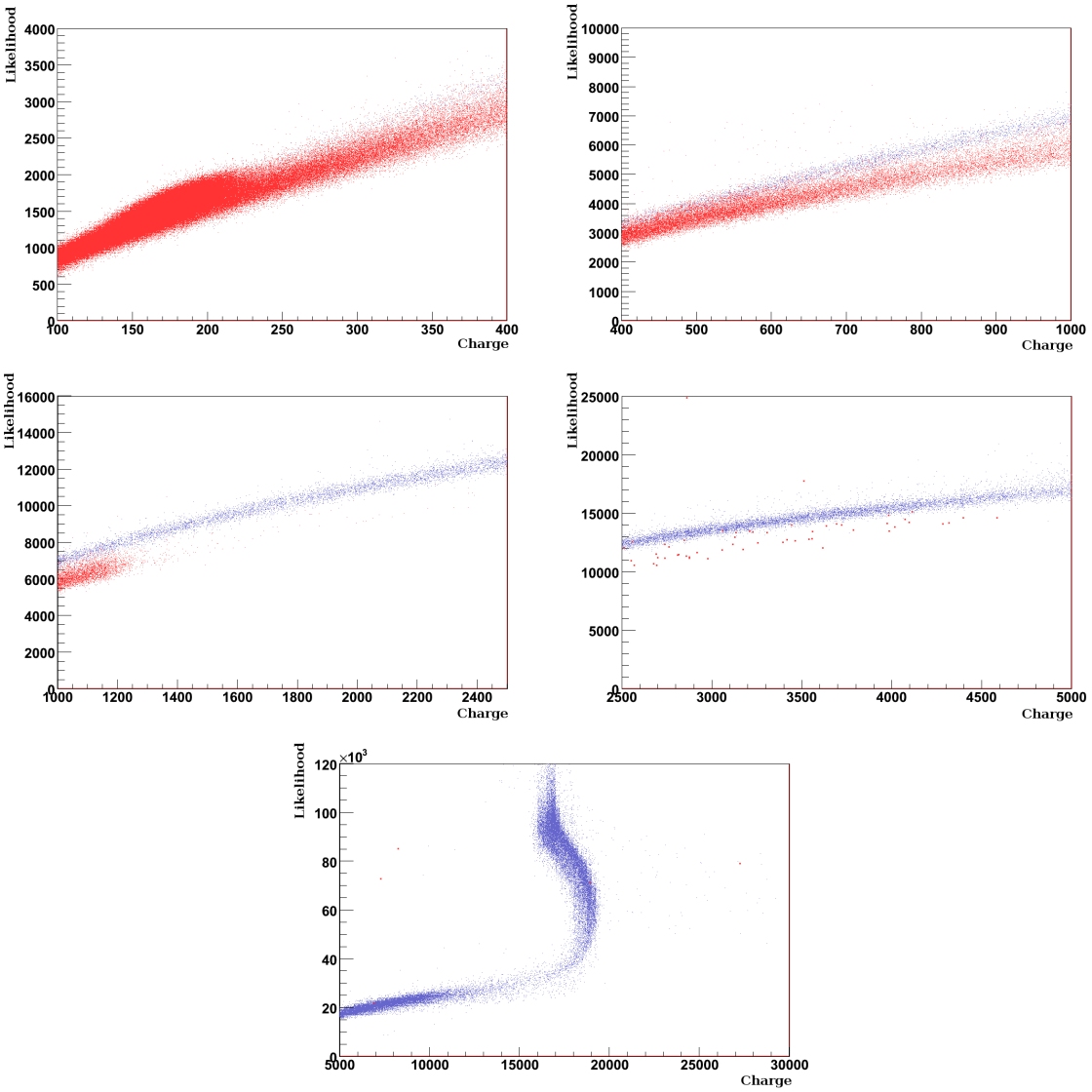

Figure 5.17: Likelihood parameter for different energy windows. Neutrino-like events shown in red, muon-like in blue. A low likelihood reflects a good event reconstruction, a large one a bad reconstruction.

by the low probability for neutrinos (just 5 remaining neutrino events). For muon-like and neutrino-like events haveing the same efficiency, the parameters for the likelihood cut are collected in Table 5.5.

5.5 Fiducial Volume

At last, the fiducial volume cut shall be mentioned. It can be applied for its own or in addition to the four cuts mentioned before. It reduces the regarded volume to the innermost,

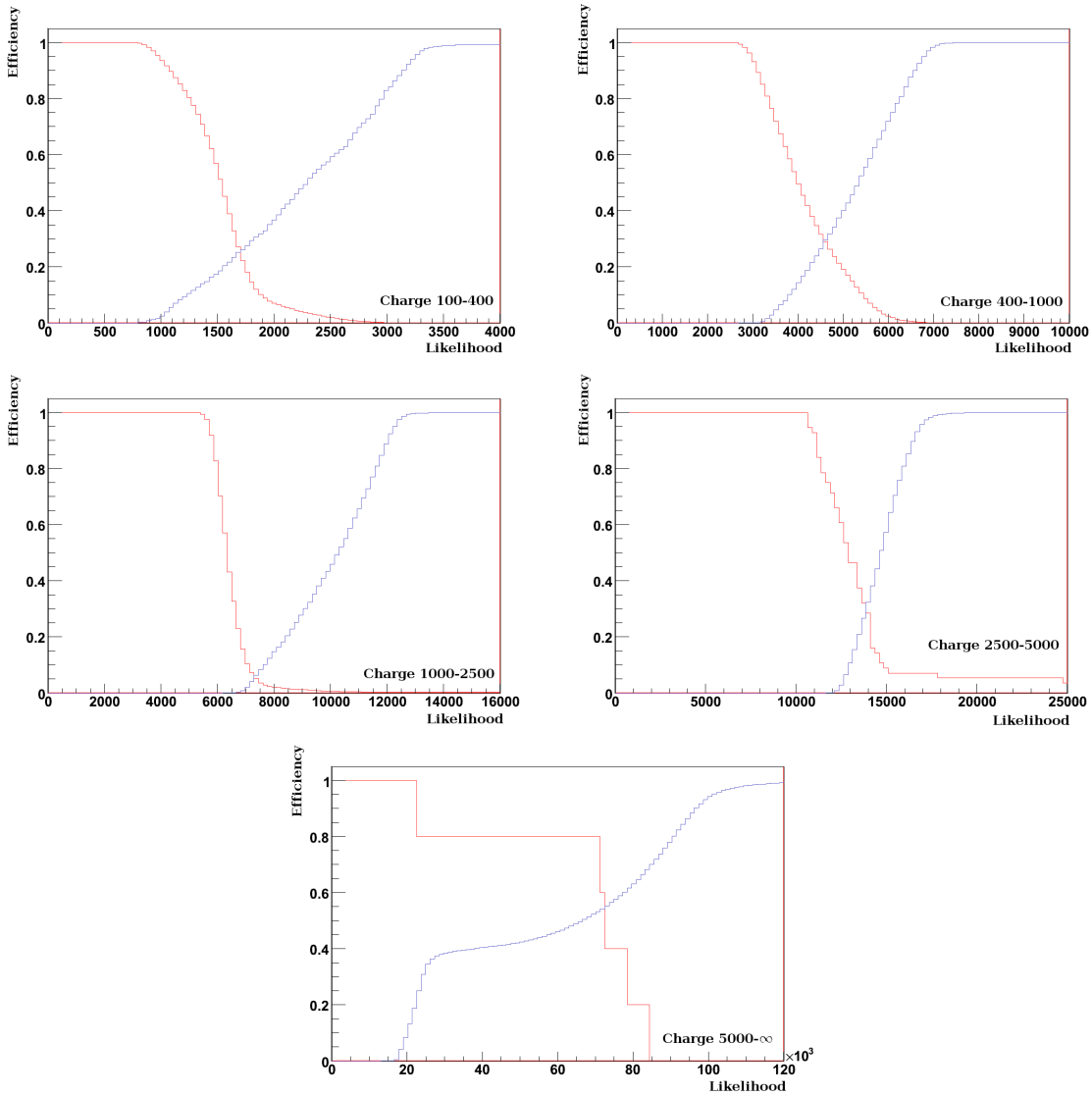

Figure 5.18: Efficiency of the likelihood cut for different energy windows. Neutrino-like events shown in red, muon-like in blue. All particles identified correctly equals 0. All particles identified as the other ones equals 1.

consisting of a sphere with a $3.5m$ radius in the Inner Vessel. The problem is, that the radius is not fixed. It depends on the used reconstruction code. The different reconstructions are not good enough (varying about 10%), but limiting the radius to these approximately $3.5m$ will do. Only low energetic muons and background radiation caused by the contamination of the surface of the Inner Vessel are prominent in the outer region. A great percentage of the muon-like events in the innermost volume are reconstructed to the outside due to their tracks. In this way mainly neutrino-like events will remain in the innermost volume.
First the fiducial volume cut is regarded for its own. Plotting the number of events versus

Energy $[MeV]$	$0.2-0.8$	$0.8-2$	$2-5$	$5-10$	$10-\infty$	$0-\infty$
Likelihood	1700	4550	7100	13900	72500	4950
Efficiency [%]	74	71	94	69	45	97

Table 5.5: Best values for the likelihood cut. Both, neutrino-like and muon-like events have the same efficiency at that point. The efficiency here gives the percentage of identifying a particle as what it is.

the charge, it can be seen that a separation of neutrino-like and muon-like events for the total energy range observed can be performed (Figure 5.19). As it can be seen regarding

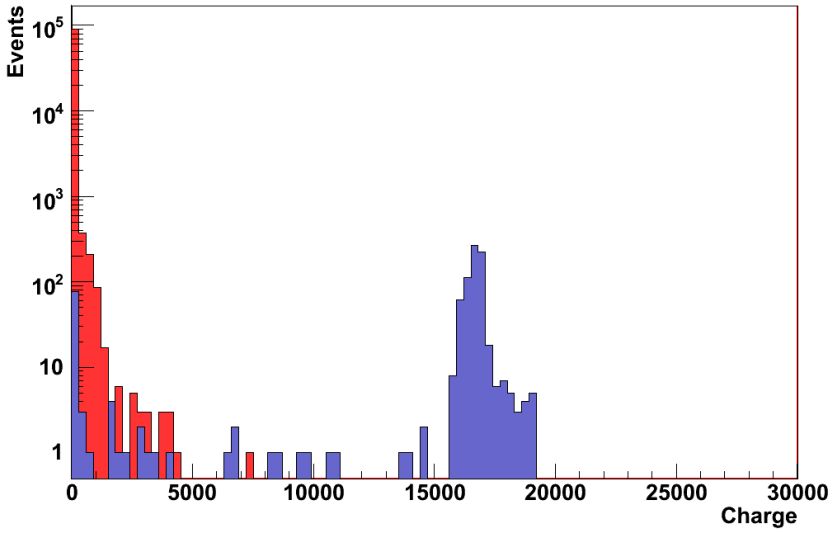

Figure 5.19: Fiducial volume cut for the total energy range observed by Borexino. Neutrino-like events shown in red, muon-like in blue.

the different energy ranges (Figure 5.20), the neutrino-like and muon-like events seperate by energy. For low energies their are almost only neutrino-like events, while for high energies only muon-like events are identified. Second, this cut can be used in addition to the other cuts, discussed before. They are all affected in the same way. Because of that it will just be demonstrated for the example of the Tail-to-Total method (Figure 5.21). The observed energy window is the total one. Muon-like events are again shown in blue, neutrino-like events in red. As can be seen the two different type of identified evnets can now be seperated very good. This is also reflected in the efficiency shown in Figure 5.22. Hence the fiducial volume cut plays an important role for data evaluation (see Chapter 2.2).

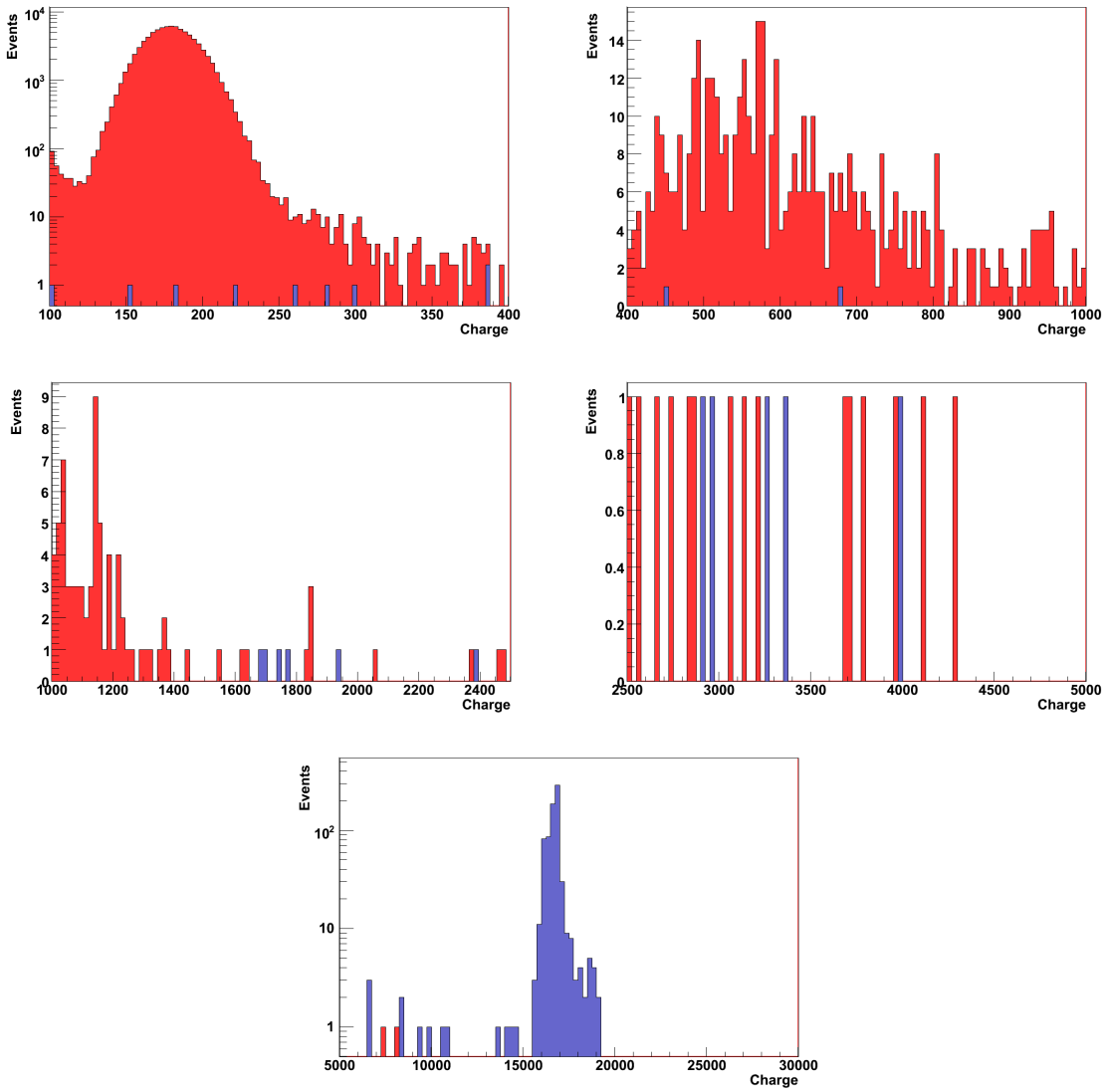

Figure 5.20: Fiducial volume cut for the different energy ranges. Neutrino-like events shown in red, muon-like in blue.

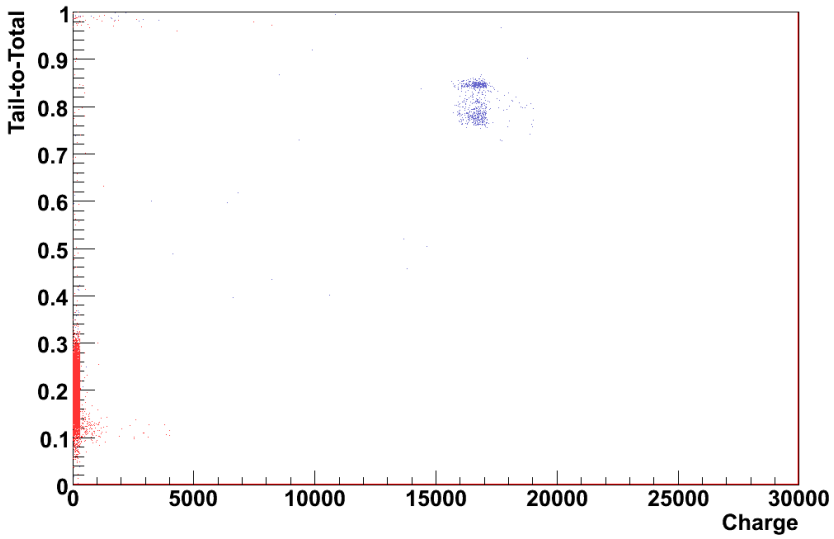

Figure 5.21: Fiducial volume cut applied to the Tail-to-Total method regarding the total energy spectrum observed by Borexino. Neutrino-like events shown in red, muon-like in blue.

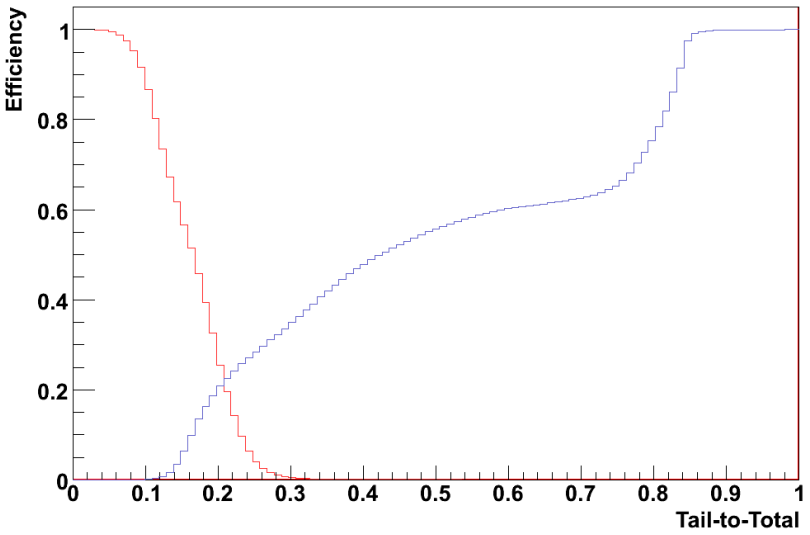

Figure 5.22: Efficiency of the fiducial volume cut applied to the Tail-to-Total method for the total energy range. Neutrino-like events shown in red, muon-like in blue. All particles identified correctly equals 0. All particles identified as the other ones equals 1.

6 Efficiency of the Muon Veto

As mentioned before, it is important to be able to identify the muons precisely. Especially at high energies, the radioactive background of the measured spectrum is influenced by muons, as could be seen for the data evaluation (see Section 2.2). Therefore, in this chapter the efficiencies of the Inner and Outer Muon Veto are determined. At first the Inner Veto is discussed, combining the various possible cuts described in Chapter 5. Next, the efficiency of the Outer Muon Veto will be determined. At last a short overview of combining both vetos will be given.

6.1 Inner Veto

The aim of a high probability of muon identification can be achieved by combining the cuts on different parameters. Of course, the loss of neutrino-like events is tried to be kept as low as possible. There are two different possibilities to combine the single cuts.

1. **and**: All four cuts have to be applied at once. Each cut has to identify the muon. In order to get a high efficiency for muon-like event identification, the combined efficiency for identifying a neutrino-like event will be as bad as the worst single efficiency of the cuts applied. This will not enhance the quality of the cuts. So this method will not be applied.

2. **or**: Just one of the four cuts has to identify a muon-like event to identify it in total as a muon. The efficiency for muon identification is independent of the single cut and can rise to high values. At the same time other cut parameters can be lowered, so that a higher efficiency for neutrino-like event identification will result. This method is able to rise both efficiencies, for muon-like event identification and neutrino-like event identification. Therefore this is the better choice to combine the different cuts.

In this way the efficiency of muon detection can be increased to a level of 99.9%. It was also considered to set a higher value, but after first results were present, the loss of neutrinos was decided as too high. The identification of particles with the Outer Detector was used again as reference (see Chapter 5). The different energy windows were treated independently of each other. The best cut was determined by setting the efficiency of the cut to 99.9%, while the loss of neutrinos stays minimal. The results for the cut parameters are gathered in Table 6.1. The amount of neutrinos and muons detected via the combined cuts is also presented there. The same procedure was repeated, using the fiducial volume cut in addition. These results can be seen in Table 6.2 The miss-identification of neutrinos and muons in the energy window $10 - \infty$ can be related to the inefficiency of the Outer Detector. The low rates for neutrino detection in the total energy spectrum $0 - \infty$ are due to the imprecise linear fit that determines the cut parameters, distinguishing between neutrino-like and muon-like events.

Energy $[MeV]$	$0.2-0.8$	$0.8-2$	$2-5$	$5-10$	$10-\infty$	$0-\infty$
Deutsch-Parameter	0.164	0.152	0.152	0.164	0.156	0.132
PeakTime $[ns]$	4.2	14.7	/	20.3	36.4	10.5
Tail-to-Total	0.12	0.15	0.15	0.17	0.81	0.22
Likelihood	3600	6000	8400	15600	74400	6000
Muons by OD	948	3379	5659	9248	34835	54196
Muons by cuts	337397	8972	5979	9251	34818	297441
Neutrinos by OD	377102	24645	3663	56	5	424689
Neutrinos by cuts	40653	19052	3343	53	22	181444

Table 6.1: Detection rates and cut parameters of all cuts combined except the fiducial volume cut. Covering the different energy windows introduced in Chapter 5.

Energy $[MeV]$	$0.2-0.8$	$0.8-2$	$2-5$	$5-10$	$10-\infty$	$0-\infty$
Deutsch-Parameter	0.24	0.412	0.264	0.236	0.152	0.132
PeakTime $[ns]$	21.0	16.1	19.6	21.0	35.7	8.4
Tail-to-Total	0.47	1.00	1.00	0.68	1.00	0.27
Likelihood	3600	76800	60000	18000	87600	3600
Muons by OD	9	2	6	5	737	829
Muons by cuts	112	9	9	8	739	49349
Neutrinos by OD	88486	522	81	16	2	90670
Neutrinos by cuts	88383	515	78	13	0	42150

Table 6.2: Detection rates and cut values of all four cuts combined in addition with the fiducial volume cut. Covering the different energy windows introduced in Chapter 5.

Because this was already assumed to happen, the different energy ranges were regarded separately. For smaller energy windows, the detection rates could further be increased.

6.2 Outer Veto

Next, the efficiency of the Outer detector was determined. Therefore the neutrinos and muons flagged by the Outer Veto are compared to the results generated by the different cuts introduced in Chapter 5. It is regarded how many muons have been flagged as neutrinos, so the efficiency of muon detection can be calculated. To make the decision, if the event really is a neutrinolike or a unidentified muon as simple as possible, the energy window starting from $10MeV$ is observed as there are no more radioactive background events and a negligible low neutrino rate left. Figure 6.1 shows the Deutsch-Parameter used for the data of the Outer Muon Veto, identifying muonlike (blue colour) and neutrinolike (red color) events. Now it must be determined if the neutrinos shown here really are neutrinos or not. In the shown case, there are two arguments why the neutrinos are more likely to be muons.

1. The energy window observed is very high. It is unlikely that there are any neutrinos

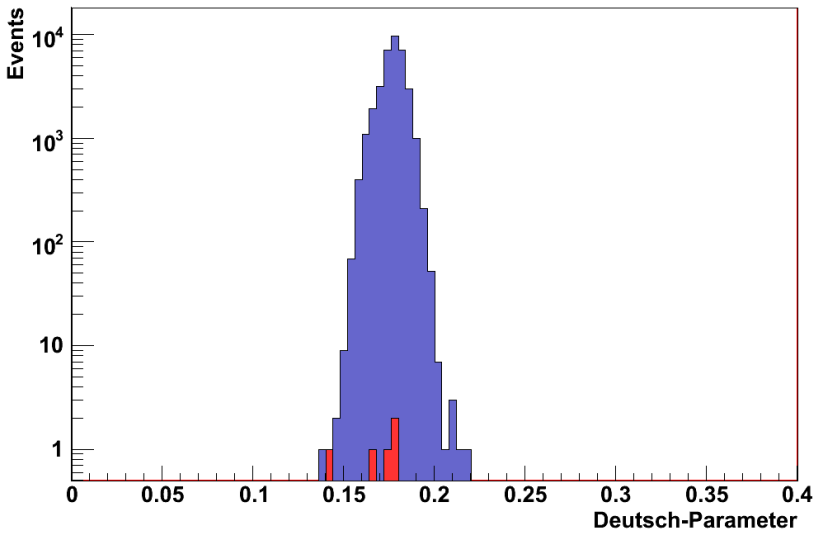

Figure 6.1: Efficiency of the outer detector. The neutrinos shown in red are most likely muons (shown in blue), as they follow the distribution of muon events using the Deutsch-Parameter cut.

in that range

2. Regarding the Deutsch-Parameter, it can be seen that the neutrinos are all following the distribution of muon events.

Therefore it is very likely that the 5 (out of 34840 events) particles detected as neutrinos are muons that have not been flagged by the Outer Detector. The same result is achieved with the other three cuts. The results are collected in Table 6.3. As it can be seen, the

Cut	Deutsch	Mean-PeakTime	Tail-to-Total	Likelihood
Events in total	34840	34840	34840	34840
Wrong identified	5	5	5	5

Table 6.3: Wrong flagged events, detected by the Outer Muon Veto. Determined using the different cuts for energies above $10MeV$.

result is independent of the different cut used. The efficiency ϵ of the Outer Muon Veto adds up to at least

$$\epsilon \geq 99.985649\% \pm 0.006418\%(stat.) \tag{6.1}$$

as the miss-identified particles could be neutrinos anyway.

6.3 Combined Efficiency

Now, that the efficiencies of the Inner and Outer Moun Veto have been determined, the efficiency of detecting a moun with the combined muon vetos can be calculated. Because the two veto systems are working independent of each other the efficiency of the Outer Detector and the 99.9% of the inner veto can be combined. The total efficiency adds up to:

$$\epsilon_{total} = 99,999999\% \pm 0,006424\%(stat.) \tag{6.2}$$

What has to be sacrificed is the neutrino event rate, as already mentioned. For the different energy ranges, the loss of neutrinos is summed in Table 6.4. As it can be seen, the loss of

Energy $[MeV]$	$0.2-0.8$	$0.8-2$	$2-5$	$5-10$	$10-\infty$	$0-\infty$
Neutrinos lost, no fiducial volume cut [%]	89.22	22.70	8.79	10.71	80.00	57.28
Neutrinos lost, with fiducial volume cut [%]	0.12	1.34	3.70	18.75	100.00	53.51

Table 6.4: Percentage of neutrinos lost for the total efficiency

neutrinos with the applied fiducial volume cut is by far not so high as without. The high rates for the energy range $10-\infty$ refer to the inefficiency of the Outer Detector, as already mentioned. Using the combined cuts, especially in addition with the fiducial volume cut, the detected neutrino event rate is just slightly influenced. Hence there are no new effects on the results due to underground radiation.

7 Summary and Outlook

By now a lot of solar neutrino experiments have validated the predictions of the Standard Solar Model. It was able to measure neutrino mixing and upper limits for neutrino masses were determined. But untill the beginning of 2007 no project was able to do a realtime measurement of the ^7Be neutrino flux component. Now, with a full serviceable Borexino experiment, this has been done. First measurements already could announce a ^7Be neutrino rate of $47 \pm 7(stat.) \pm 12(syst.) \frac{counts}{100t \cdot day}$, with still a quite high systemetical and statistical error. In the future, with a longer exposure time and better event reconstructions the obtained data will become more precise.

In order to keep Borexino a well working detector, the hardware system has to be checked as often as possible. Therefore a pulser system for the Outer Detector was installed, injecting a reference signal. The developed software makes it possible to distinguish between defect PMTs or defect QTC-channels. Therefore a quick reparation of the problem can be performed. In the future addons can be included to this module, as it is planned to develope a determination procedure for channel delays of the outer detector, that can be used for callibration of the respective channel.

To verify the measured data a simulation program is used. It simulates a neutrino or muon hit that can be evaluated with the normal data evaluation software Echidna. The gained data sample can be compared to real acquired data. This simulation program was just available for the Inner Detector. During this thesis, the program was extended to the Outer Detector. The simulated data can be used to verify a muon track reconstruction program for the Outer Detector. Further, a comparison with normal data can be performed. A last overall check for the simulation is scheduled within the next month. In the future, the trigger system for the Outer Detector is planed to be included into the simulation code, too.

As mentioned before, it is of great interest to identify muons hitting the detector, in order to exclude them from the neutrino spectrum. Therefore different cuts have been considered in this thesis. As it was shown, it is possible to distinguish between neutrinolike and muonlike particles using the Deutsch-parameter, peaktime, tail-to-total ratio and the likelihood as well as the fiducial volume cut. In the future the different energy ranges observed could be limited to smaller windows. A more precise cut between neutrinolike and muonlike events could be performed in that way.

In the last chapter the single cuts mentioned before were combined. Achieving a muon identification efficiency of 99.9% for the Inner Detector with a minimum of neutrino missidentification was the purpose. It was observed that the neutrino rate is dependant on the regarded energy window.
Using the different cuts for high energy regions, the efficiency of the Outer Detector could

be determined to approximately 99.986%.
Combining both vetos, an even better total efficiency is achieved. The loss of neutrinos is dependent on the observed energy region, but in general their rate remains well. Therefore the results for neutrino observations should only be slightly influenced. For future analysis, the neutrino detection rate could be enhanced, regarding smaller ernergy windows for the cuts and therefore getting better parameters.

For Borexino being just at the beginning of data acquisition a lot of work will have to be done in the future. Antineutrino observation as well as geoneutrino observation is planned. It is discussed to build a muon track reconstruction device ontop of the Outer Detector to compare these results with the ones generated by the muon track reconstruction program.

List of Figures

List of Tables

Bibliography

[BahWP] John Bahcall's viewgraph website:
http://www.sns.ias.edu/∼jnb/SNviewgraphs/snviewgraphs.html, 01.11.2007

[Bor02] Borexino Collaboration:
Science and Technology of BOREXINO: A Real Time Detector for Low Energy Solar Neutrinos, Astropart Phys. 3, p. 205-234 (2002)

[Bor07] Borexino Collaboration:
First real time detection of ^{7}Be solar neutrinos by Borexino, astro-ph 0708.2251v1

[BorWP] Official Borexino homepage:
http://borex.lngs.infn.it, 13.11.2007

[Cuore] I. G. Irastorza, A. Morales S. Scopel and S. Cebrián:
Physics Potential and Prospects for the CUORICINO and CUORE experiments, arXiv:hep-ph/0108146v3 17 Jun 2002

[DDa06] Davide DAngelo:
Towards the detection of low energy solar neutrinos in BOREXino: data readout, data reconstruction and background identification; Dissertation, Technische Universität München, 2006

[FukYa] M. Fukugita and T.Yanagida:
Physics of Neutrinos and Applications to Astrophysics, Springer 2003

[Gal98] Michael Altmann:
GALLEX solar neutrino observations: Results from the total data set
Invited talk at the "XXXIIIrd Rencontres de moriond: Electroweak Interactions and Unified Theories", Les Arcs (France) March 14-21, 1998

[GNO05] GNO Collaboration:
Complete results for five years of GNO solar neutrino observations, Phys.Lett. B616 (2005) 174-190, arXiv:hep-ex/0504037

[Hom98] Bruce T. Cleveland, Timothy Daily, Raymond Davis, Jr., James R. Distel, Kenneth Lande, C. K. Lee, Paul S. Wildenhain and Jack Ullman:
Measurement of the solar electron neutrino flux with the Homestake Chlorine Detector, The Astrophysical Journal, 496:505-526, March 20, 1998

[Kam02] KamLAND Collaboration:
First Results from KamLAND: Evidence for Reactor Anti-Neutrino Disappearance, arXiv:hep-ex/0212021v1 9 Dec 2002

[Kam03] KamLAND Collaboration:
A High Sensitivity Search for $\overline{\nu}_e$s from the Sun and Other Sources at KamLAND, arXiv:hep-ex/0310047 v1 23 Oct 2003

[Kam04] KamLAND Collaboration:
Measurement of Neutrino Oscillation with KamLAND: Evidence of Spectral Distortion, arXiv:hep-ex/0406035v3 1 Nov 2004

[Kam07] Itaru Shimizu:
Present Status and Future Prospects of KamLAND, The International Workshop on Double Beta Decay and Neutrinos, Jun. 12, 2007

[Kam96] Kamiokande Collaboration:
Solar Neutrino Data covering Solar Cycle 22, Phys. Rev. Lett., vol. 77, p. 1683, (1996)

[KatHp] KATRIN homepage:
http://www-ik.fzk.de/∼katrin/index.html, 6.11.2007

[KatLi] A. Osipowicz et al.:
Letter of Intent: KATRIN: A next generation tritium beta decay experiment with sub-eV sensitivity for the electron neutrino mass

[Lud05] Ludwig Stefan Niedermaier:
High Efficiency Purification of Liquid Scintillators for the Solar Neutrino Experiment Borexino; Dissertation, Technische Universität München, 2005

[Min06] The MINOS Collaboration:
Observation of muon neutrino disappearance with the MINOS detectors in the NuMI neutrino beam, arXiv:hep-ex/0607088 v2 29 Jul 2006

[Minos] MINOS Homepage:
http://www-numi.fnal.gov, 6.11.2007

[NASA] NASA's Imagine the Universe:
http://imagine.gsfc.nasa.gov/docs/science/know_l2/sun_parts.html, 05.11.2007

[NNN07] Davide DAngelo:
First real time ^{7}Be solar ν detection in Borexino, talk: NNN07-Hamamatsu

[Povh] Povh,Rith,Scholz and Zetsche:
Teilchen und Kerne, Springer 2004

[Sag02] The SAGE Collaboration:
Measurement of the Solar Neutrino Capture Rate by the Russian-American Gallium Solar Neutrino Experiment During One Half of the 22-Year Cycle of Solar Activity, arXiv:astro-ph/0204245v2 9 Jul 2002

[SNO06] The SNO Collaboration:
Measurement of the ν_e and Total ^8B Solar Neutrino Fluxes with the Sudbury Neutrino Observatory Phase I Data Set, arXiv:nucl-ex/0610020 v1 13 Oct 2006

[SNO99] The SNO Collaboration:
The Sudbury Neutrino Observatory, arXiv:nucl-ex/9910016 v2 3 Nov 1999

[SuKa2] The Super-Kamiokande Collaboration:
The Super-Kamiokande Detector, 6. December 2002

[SuKa5] The Super-Kamiokande Collaboration:
Solar neutrino measurements in Super-Kamiokande-I, arXiv:hep-ex/0508053v2 26 Sep 2005

[Tau07] Marco Pallavicini
Getting the first $^7Be\nu$ detection: scintillator purification, detector response and data analysis in Borexino, Taup 2007

[WikNe] Wikipedia website:
http://en.wikipedia.org/wiki/CNO_cycle, 30.10.2007

Acknowledgements

First I want to thank Prof. Franz von Feilitzsch for giving me a warm welcome and the possibility to be at his chair.

Next my gratitude goes to Prof. Lothar Oberauer for giving me this very interesting thesis, that made it possible for me to get a very fascinating view on astroparticle physics. Also for not professional conversations relaxing the situation thanks must be applied.

I would like to thank Michael Wurm who was a good supervisor to me especially for not getting tired when being questioned. His good introduction to the subject made work much easier.

Especially for the introduction to Root and for many fruitful discussions Teresa Marrodán Undagoitia must be thanked.

Great thanks to Beatrice van Bellen and Alexandra Füldner for their friendly kind and for helping me with several formulars and paperwork.

All the other members of the E15 chair must be thanked for the good working condition and lots of nice discussions, not only in the professional sector.

Thanks to all the members of the Borexino Collaboration for giving me a warm welcome. Especially to Davide D'Angelo who supervised me during my work at LNGS.

Special thanks go to my brother. He supported me in bad times and was always there if I needed help or something else. Therefore great thanks.

Most important my parents. They always helped and supported me. Without them all the work I have done so far wouldn't be possible. Thanks a lot for all the love over all the years.